


Properties of warm absorbers in active galaxies: a systematic stability curve analysis

Susmita Chakravorty¹ , Ajit K. Kembhavi¹, Martin Elvis², Gary Ferland³

¹*IUCAA, Post Bag 4, Ganeshkhind, Pune 411 007, India;*

²*Harvard-Smithsonian Center for Astrophysics, Cambridge, MA 02138;*

³*Department of Physics and Astronomy, University of Kentucky, Lexington, KY 40506*

21 February 2024

ABSTRACT

Signatures of warm absorbers are seen in soft X-ray spectra of about half of all Seyfert 1 galaxies observed and in some quasars and blazars. We use the thermal equilibrium curve to study the influence of the shape of the ionizing continuum, density and the chemical composition of the absorbing gas on the existence and nature of the warm absorbers. We describe circumstances in which a stable warm absorber can exist as a multiphase medium or one with continuous variation in pressure. In particular we find the following results: i) the warm absorber exists only if the spectral index of the X-ray power-law ionizing continuum > 0.2 and has a multiphase nature if 0.3 , which interestingly is the spectral index for most of the observed Seyfert 1 galaxies; ii) thermal and ionization states of highly dense warm absorbers are sensitive to their density if the ionizing continuum is sufficiently soft, i.e. dominated by the ultraviolet iii) absorbing gas with super-Solar metallicity is more likely to have a multiphase nature; iv) the nature of the warm absorber is significantly influenced by the absence of iron and associated elements which are produced in the later stages of star formation history in supernovae of type Ia.

Key words: quasars: absorption lines - galaxies : active - Seyfert - ISM: abundances X-rays: ISM

1 INTRODUCTION

Absorption due to highly ionized Oxygen and elements of similar atomic number (e.g. O VII, VIII, Ne X) is commonly found in the soft X-ray spectra of active galactic nuclei (AGNs) (Halpern 1984; Nandra & Pounds, 1994; Reynolds, 1997; George et al.: 1998). High resolution X-ray spectra from *Chandra* and *XMM-Newton* show that these absorption lines are always blue-shifted compared with the emission lines and so must be in outflow from the central continuum source (Collinge et al.: 2001, Kaastra et al.: 2002, Kinkhabwala et al.: 2002, Blustin et al.: 2003, Krongold et al.: 2003, Netzer et al.: 2003, Turner et al.: 2004). The absorption edges and lines respond to variation of the ionizing continuum emitted by the central engine. For example, Krongold et al. (2007) show that for NGC4051 the ionization state of the WA responds to the continuum flux as predicted for gas that stays close to photoionization equilibrium, so that other factors, e.g. velocity changes and shocks, do not appear to be important. It is therefore reasonable to assume that the absorbing cloud is photoionized by the continuum radiation from the active galactic nuclei (AGN). This partially ionized

optically thin gas along the line of sight to the center of the AGN has come to be known as the warm absorber (hereafter WA).

Understanding the structure of the WA will lead to better understanding of the structure of AGNs; for example, identifying the location from which the wind arises will impose constraints on the physics of the wind source. Some authors find that the WA is well fitted with a model with two ionization phases (Krongold et al.: 2003; Krongold et al.: 2005a; Ashton et al.: 2006; Collinge et al.: 2001) or three phases (Netzer et al.: 2003; Morales, Fabian & Reynolds, 2000; Kaastra et al.: 2002), in which the components are in pressure equilibrium. Other authors (Ogle et al.: 2004) and Steenbrugge et al.: (2005) have argued in favor of a continuous distribution of ionization state for the WA, in objects for which others fit just a few phases. One way to investigate which solution is more likely is to investigate the physics determining the thermal structure of WA.

The effect of various factors on the WA can be studied conveniently using the thermal equilibrium curve (hereafter referred to as the *stability curve*) of temperature (T) against the ratio of ionization parameter (ξ , see below for definition) to T. Gas lying off the stability curve will cool or heat until reaching the curve. If the curve has kinks that produce multiple stable values at fixed $\xi = T$, then the WA can have multiple phases in mutual equilibrium. This

[?] E-mail: susmita@iucaa.ernet.in (SC); akk@iucaa.ernet.in (AK); elvis@head.cfa.harvard.edu (MA); gary@pa.uky.edu (GF)

effect may be responsible for the multiphase nature of the interstellar medium of galaxies (Field, 1965). Ionizing continuum from AGN can induce such kinks (Krolik, McKee & Tarter, 1981), to a larger extent than the interstellar medium. The pronounced *kinks* representing WA in the stability curve lie in the intermediate temperature range, $5 < \log T < 7$ where photoionization heating and collisional cooling of various metals are expected to determine the thermal balance of the WA. The details of the thermal stability is strongly affected by the shape of the ionizing continuum emitted by the central source (i.e. their spectral energy distributions or SEDs), and by the chemical composition of the absorbing gas.

Our main motivation in this paper is to improve on previous work (Hess, Kahn & Paerels 1997; Komossa & Mathur 2001; Krolik, McKee & Tarter 1981, Krolik & Kriss 2001; Reynolds & Fabian 1995; Rozanska, Kowalska & Goncalves 2008) by carrying out a systematic investigation of the stability curves and finally to give a quantitative handle on the relative stability nature of the WA as a function of the various physical parameters involved. In Section 2 we discuss the physical properties of the WA. In Section 3 we give all the constraints and assumptions used in the paper. The simulations of the stability curves are sensitively dependent on the underlying atomic physics used by the photoionization codes. We have shown (Chakravorty et al., 2008, hereafter Paper I), that dielectronic recombination rate coefficients have a large effect on the stability curve. Using recent atomic physics databases that include many more of these rates, with more accurate values, is important because it significantly changes the predictions for the physical nature of the WA. The serious impact of this effect is addressed in further details in Section 4 while we discuss the stability curve and comparison with earlier works. We choose a specific scheme to represent the ionizing continuum (discussed in Section 3) and vary its parameters to create a reasonable ensemble of spectral shapes as demonstrated by a wide variety of AGN which harbour WA. The effect of these different SEDs on WA nature is discussed in Section 5. Rozanska et al. (2008) have demonstrated that for sufficiently soft AGN SED, the thermal balance becomes dependent on the density values if it is above a certain threshold. This can only happen if the gas is dense enough and the ionizing continuum is appropriate to induce heating processes other than photoionization to dominate the thermal balance. Since we sample a rather large variety of ionizing continua for our investigations, the present work gives us an appropriate opportunity to study the effect of density on stability curves in Section 6. Optical and ultraviolet emission and absorption line studies suggest that central regions of AGN have solar or higher metallicities (Hamann & Ferland, 1999) and the WA temperature range of the stability curve is sensitive to the atomic interactions due to various metals. This abundance dependence provides the motivation for our study of the influence of individual elements, and groups of elements in Section 7. The improved updated atomic database used for the simulations provides the opportunity to go beyond the qualitative discussions and, for the first time, make quantitative comparisons of the multiphase nature and the robustness of the stability regions as a function of the ionizing SED and chemical composition of the absorber in Section 8. Our results are summarised in Section 9.

2 WARM ABSORBERS

Studies of WA variability in response to continuum changes show that it is reasonable to assume the WA to be in ionization and thermal equilibrium (Nicastro et al., 1999). The timescales to reach

equilibrium seem to be less than a day (Nicastro et al.: 1999; Krongold et al.: 2003; Krongold et al.: 2005a; Krongold et al.: 2005b; Krongold et al.: 2007). Equilibrium is reached when photoionization is balanced by recombination, and ionization and Compton heating are balanced by recombination and Compton cooling. The Compton heating and cooling become important at high temperature which is solely determined by the shape of the illuminating continuum, and typically is $T \sim 10^7$ K for standard Seyfert 1 spectral energy distributions, which the clouds can attain only when the ionizing continuum has significant number of hard X-ray photons. The typical column density in WAs, estimated mainly using absorption edges, is $N_H \sim 10^{22} \text{ cm}^{-2}$ (see the references in Section 1). In some cases lines are easily detected whereas edges are not seen (Kaastra et al.: 2002; Rozanska et al.: 2004). However, the N_H values derived from edges alone are systematically high by large factors (~ 10) - see Krongold et al.: 2003, Kaspi et al.: 2002. Modeling of the absorber allows the temperature and ionization parameter to be calculated. Typically, the temperatures are of the order of 10^5 K and the ionization parameter ~ 100 (see definition of ξ below). However, in some objects WAs are found to have additional components which exhibit higher temperatures, 10^6 K (see the references in Section 1).

The estimated distance of the WA from the central source covers a wide range: from the kiloparsec scale of the extended narrow emission line region (Kinkhabwala et al.: 2002), through distances of $\sim 0.01 \text{ pc}$, i.e., at the scale of the obscuring molecular torus (Krolik & Kriss, 2001; Crenshaw et al.: 2003; Blustin et al.: 2005), to within the $H\beta$ broad emission line region, on the scale of the accretion disk, which is a few thousand Schwarzschild radii (Krongold et al.: 2007), where the WA would form the base of an accretion disk wind (Murray & Chiang 1995, Elvis 2000). The photoionization state of the WA can be parametrised by the ionization parameter which is the ratio of the ionizing photon flux to the gas density (Tarter, Tucker & Salpeter, 1969):

$$\xi = L_{\text{ion}} / n_H R^2 \quad [\text{erg cm s}^{-1}]; \quad (1)$$

where L_{ion} is the luminosity between $1 \sim 10^3$ Rydberg. Hence $\xi = T / L = p R^2$, p being the gas pressure in the WA. Although, in this paper we have used ξ for all our discussions, in the context of warm absorbers, there is another popular definition of the ionization parameter given by

$$U = Q_{\text{ion}} / 4 \pi c n_H R^2; \quad (2)$$

Q_{ion} (s^{-1}) is the rate of incident photons above 1 Rydberg and c is the velocity of light. For a given shape of the SED of the ionizing continuum, the conversion from ξ to U is unique and can be done conveniently. Although luminosity can be constrained from separate independent observations, it is difficult to remove the degeneracy between density and distance in the product $n_H R^2$ featuring in the denominator of the ionization parameter. Thus, the estimation of distances for WA becomes challenging; for example, Netzer et al. 2003 and Krongold et al. 2006 put upper limits differing by up to three orders of magnitude on the WA distance in the same object NGC3783 (but using different observations). As the mass loss rate is proportional to the radius such large factors of uncertainty have a large effect on AGN energetics and on feedback from the AGN to the surrounding media.

Krolik, McKee and Tarter (1981) showed that a stable state exists at $T \sim 10^4$ K for a photoionized cloud which undergoes collisional cooling. There can be an additional stable state for the absorbing cloud at $T \sim 10^8$ K, if the incident photoionizing continuum has a hard X-ray component as an extra heating agent. Thus

they suggest that presence of a hard X-ray continuum would result in clumping, with cold clouds remaining in equilibrium with a hot medium. However, for optically thin, ionized gas, the temperature range $10^5 - 10^7$ K is well known to be an unstable zone, bringing into question the model of WA as gas in thermal equilibrium. Radiation in spectral lines is the primary cooling mechanism in this temperature range. The contribution from radiative recombination and two-photon continuum emission (Gehrels & Williams 1993) form some additional small regions of stability.

3 CONSTRAINTS AND ASSUMPTIONS

3.1 The code and its implementation

We assume a simple model of a geometrically thick, optically thin, plane parallel slab of gas illuminated on one face for the absorbing medium which is located at a certain distance R from a central continuum source of bolometric luminosity L . The geometrical thickness of the gas is taken to be much less than R . The physical condition of the absorbing medium is determined by the flux received at the illuminated face of the gas ($L=4\pi R^2$), the shape of the ionizing continuum (SED), the number density of the gas n_H , the column density of the gas N_H , and the chemical composition of the absorbing gas. To obtain the equilibrium conditions for a gas with an assumed set of parameters which specify these inputs, we have used the publicly available photoionization code `CLOUDY`¹ version C07.02 (hereafter C07), see Ferland (1998).

`CLOUDY` calculates the ionization equilibrium conditions by solving the energy and charge conservation equations under the assumption that all the atomic processes have had time to reach a steady state. The density n_i of i^{th} species is then given by the balance equation

$$\frac{dn_i}{dt} = \sum_{j \neq i} n_j R_{ji} + \text{Source} - n_i \left(\sum_{j \neq i} R_{ij} + \text{Sink} \right) = 0; \quad (3)$$

where R_{ji} is the rate of species j going to i , Source is the rate per unit volume of appearance of new atoms in i^{th} species and Sink is the rate that they are lost (Osterbrock & Ferland, 2006). Thermal equilibrium conditions are calculated by evaluating the heating and cooling rates at different temperatures for the given gas and finding the temperatures where the two rates balance each other.

For all the calculations in this paper we have used `CLOUDY` in the *constant density* mode which is chosen for the sake of numerical simplicity, as we probe a rather large range of parameter space to determine the properties of the WA. We would like to note here that using the TITAN code (Dumont, Abrassart & Collin, 2000), Rozanska et al. (2006) and Goncalves et al. (2006) have pioneered the *constant total pressure* mode of calculations for photoionization equilibrium where they relax the approximation that the density is constant. Their only assumption is that the line of sight gas is in total pressure equilibrium and they introduce additional iterations between temperature and density within the code in a self consistent manner. This results in natural stratification of the cloud with different temperatures and densities where each layer is illuminated

by the radiation already absorbed by the previous layer. These two methods agree well with each other for optically thin clouds, but show significant differences when the column density of the absorbing cloud is high ($N_H \gtrsim 10^{22}$). In our future publications where we will restrict ourselves to study equilibrium properties of WA as functions of a smaller range of physical parameters, we will use similar methods.

3.2 Density dependence

Estimation of temperature is independent of n_H , for a gas in thermal and ionization equilibrium when the dominant processes of heating and cooling are photoionization and recombination respectively. This is because in this regime of thermal equilibrium, density enters the temperature estimation only through the ionization parameter. Hence the stability curve would be insensitive to the value of the density used. This gives us the liberty to choose an intermediate value for WA density, $n_H = 10^9 \text{ cm}^{-3}$, leading to $L=R^2 \cdot 10^{11}$ from Equation 1, for typical values ~ 100 corresponding to WA. Except for Section 6, where we check the robustness of this assumption, we have assumed the value 10^{11} for $L=R^2$ throughout the paper.

3.3 Ionizing continuum

The 1–10 keV part of the observed spectra of AGN is usually modeled as a simple power-law with exponential lower and upper cut-offs specified by E_{min} and E_{max} respectively,

$$f(\nu) = e^{-\frac{E_{\text{min}}}{h\nu}} e^{-\frac{E_{\text{max}}}{h\nu}}; \quad (4)$$

where $f(\nu)$ is the flux per unit frequency interval and $\nu > 0$ is the energy spectral index. For most quasars, the X-ray spectral index lies in the range $0.7 < \nu < 0.9$ as shown by Wilkes & Elvis in 1987 and also recently by Grupe et al. 2006 and Lopez et al. 2006. However some objects show extreme values like $\nu < 0$ or $\nu > 2$. There is a systematic difference between radio-quiet and radio-loud AGNs in that radio-quiet AGNs have steeper X-ray spectra ($\nu \sim 1.0$) than radio-loud ones, ($\nu \sim 0.5$, Wilkes & Elvis 1987; Grupe et al. 2006; Lopez et al. 2006).

Ionizing continua given by Equation 4 have been used earlier by Reynolds & Fabian (1995, hereafter RF95) for doing detailed analysis of nature of WA as a function of various relevant physical parameters. Their work is further discussed in Section 4. The dashed and dotted curve labeled as *Early set* in the lower panel of Figure 1 is drawn using Equation 4 with $\nu = 0.8$, $E_{\text{min}} = 13.6 \text{ eV}$ and $E_{\text{max}} = 40 \text{ keV}$.

The extension of the soft X-ray SED into the extreme ultraviolet (EUV) cannot be directly observed in most cases because energy in EUV is easily absorbed by our own Galaxy. The join between the EUV and X-ray flux is parametrized by the slope α_{ox} defined as

$$\alpha_{\text{ox}} = -0.384 \log \left[\frac{F(2 \text{ keV})}{F(2500 \text{ \AA})} \right] \quad (5)$$

(Tananbaum et al., 1979). To obtain α_{ox} in the observed range $1 < \alpha_{\text{ox}} < 2$ we need a steeper soft component in addition to the power-law given by Equation 4. We assume a two component SED to simultaneously include the information on X-ray and EUV and which can be expressed as

$$f(\nu) = \left[\frac{A}{\nu} + \frac{B}{\nu^s} \right] e^{-\frac{E_{\text{max}}}{h\nu}} \text{ for } \nu > 2500 \text{ \AA}; \quad (6)$$

¹ URL: <http://www.nublado.org/>

where $s > 0$) is the spectral index of the steep soft component and f_0 is the relative normalization factor. For energies lower than 2500\AA we have used a spectral shape given by

$$f(\nu) = \begin{cases} \nu^{-0.5} & \text{for } 0.206 \text{ Ryd} < \nu < 2500\text{\AA} \\ \nu^{-1.0} & \text{for } 9.12 \times 10^3 < \nu < 0.206 \text{ Ryd} \\ \nu^{-2.5} & \text{for } \nu < 9.12 \times 10^3 \end{cases} \quad (7)$$

which is similar to the shape used by Mathew & Ferland (1987) for the same energies. Equation 6 and Equation 7 taken together describe a more realistic ionizing continuum which irradiates the WA. Such a continuum is shown as the solid curve labeled *Standard set* in Figure 1 with $s = 0.8$, $s_s = 2.0$, $\alpha_{ox} = 1.2$, $E_{max} = 200 \text{ keV}$ and lower energy cut-off following Equation 7.

In the lower panel of Figure 1, the *Standard set* continuum is compared with various other SEDs used or discussed in this paper and we will refer to these comparisons in more details in Section 4. In this paper we have used the simple definition for the ionizing continuum, as in Equation 4, only in Section 4 where we have given an introductory description of the stability curve and compared results with similar works in literature (RF95). In all other sections we have considered the more realistic *Standard set* spectra. All through the paper we have assumed $s = 2$, and for a given value of s , obtained the desired value of α_{ox} by adjusting s_s . In Section 5, when we investigate the changes in the nature of the stability curve with variation in the shape of the continuum, we consider a wide range of slopes, $0.2 < s < 1.1$ and $1 < \alpha_{ox} < 1.8$ and a wide range of higher energy cutoff, $50 \text{ keV} < E_{max} < 400 \text{ keV}$ to incorporate various types of AGN.

4 STABILITY CURVE AND EARLIER STUDIES ON IT

4.1 Definition

The stability curve, may be considered to be a phase diagram in the $\log T - \log(\dot{M}/\dot{M}_E)$ plane, with each point on the curve representing an equilibrium state of the system at a temperature T , for ionization parameter ξ . The other parameters describing the system have specific values as mentioned below. The solid curve in Figure 2 is generated using version C07 of *CLOUDY*, for an absorber having gas density $n_H = 10^{11} \text{ cm}^{-3}$ and solar metallicity, being ionized by a power-law continuum having energy spectral index $s = 0.8$ and extending from 13.6 eV to 40 keV ; hereafter we will refer to this as the *Early model* and the corresponding parameter set as the *Early set*. Computations were done using a grid of models with a range of values of the ionization parameter ξ , and the code is constrained to perform single zone calculations to ensure that the gas is optically thin. The ionizing continuum used in the *Early model* is shown as the dotted-and-dashed curve in the lower panel of Figure 1. We use the *Early set* in this section to compare results with earlier works like RF95 who have done extensive study of the stability properties of the WA as a function of various shapes of the ionizing continuum.

An isobaric perturbation of a system in equilibrium is represented by a small vertical displacement from the stability curve; such perturbations leave $\dot{M}/\dot{M}_E = L/pR^2$ constant, which for constant L/R^2 leave the pressure unchanged. If the system is located on a part of the curve with positive slope, then a perturbation corresponding to an increase in temperature leads to cooling, while a decrease in temperature leads to heating of the gas. A gas in such a state is therefore thermally stable. On the other hand, a gas located in a region of the curve with negative slope is thermally unstable,

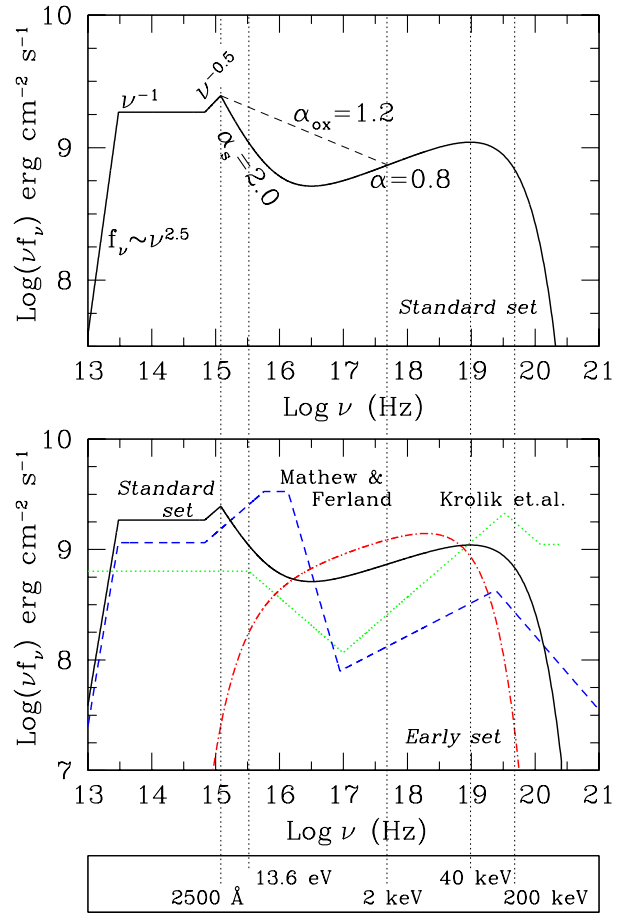


Figure 1. Top panel : Ionizing continuum obtained using Equation 6 and Equation 7 taken together, where $s = 0.8$, $s_s = 2.0$, $\alpha_{ox} = 1.2$ and the continuum is exponentially cut-off at 200 keV . At lower energies, this continuum is cut-off following Equation 7 with the successive spectral indices of -0.5 ; -1.0 and -2.5 . This continuum is labeled as the *Standard set*. We have also appropriately labeled the dominant component of the SED at various energies and used the dashed line to show the resultant $\alpha_{ox} = 1.2$. Bottom panel : Comparison of the *Standard set* ionizing continuum with various other SEDs used or discussed in this paper. The dotted-and-dashed line labeled as the *Early set* is the ionizing continuum given by Equation 4 with a X-ray slope $s = 0.8$ and exponential cut-offs at $E_{min} = 13.6 \text{ eV}$ and $E_{max} = 40 \text{ keV}$. The dotted line represents the ionizing continuum used by Krolik et al.: 1981 and the dashed line that used by Mathew & Ferland (1987). The important energy values including the upper and lower energy cut-offs (13.6 eV , 40 keV and 200 keV) and the range of definition for α_{ox} (2500\AA and 2 keV) have been marked and labeled.

and may achieve a multiphase equilibrium under certain physical conditions which we will discuss in later sections.

4.2 Earlier studies

Before we go on to discuss our own results with the stability curve, here, we would like to mention some of the earlier works done by various authors on WA and/or stability curves.

Krolik et al.: (1981) obtained the stability curve for AGN using parameters similar to our *Early set* except for the ionizing

continuum. The continuum used by them is plotted as the dotted curve in Figure 1. They have argued in favour of 10^4 K stable states remaining in pressure equilibrium with the 10^8 K phases. Although there are some narrow stable phases at 10^5 K, they have ignored the significance of such states. Moreover their stability curves do not show any stable states at 10^6 K.

In a similar study on the absorbing medium, Mathew & Ferland (1987) do not find the 10^4 K and 10^8 K phases in pressure equilibrium with each other. The continuum used by Mathew & Ferland (1987) is widely used as a broad band continuum for AGN modeling studies and has been represented with the dashed line in Figure 1. The energy spectral index of the ionizing continuum in the *Standard* set is very similar to that of the Mathew & Ferland SED in X-rays (0.3 - 100 keV). However, it is not objective to make a comparison at this stage because, although the ionizing continuum in the *Standard* set given by Equation 6 represents the overall shape of the SED between 3.6 eV to 2 keV using the definition of α_x , it is unable to give information on any underlying specific features in this energy range. In this paper we will constrain ourselves to use ionizing continuum given by Equation 6 and Equation 7, but will investigate the details of the spectral shape in the energy range (1 - 1000 eV) in subsequent publications (Chakravorty et al.; in preparation) by incorporating the effect of soft excess at 150 eV and a disk blackbody component at 20 eV.

Reynolds and Fabian (1995, RF95) have studied the warm absorber stability conditions using physical conditions as described by our *Early set* of parameters. They used a simple power-law for the ionizing continuum and varied the power-law index to check for its effects on the WA and also examined some basic effects of adding a soft excess component to the power-law ionizing continuum. Using power-law continuum with $\alpha = 0.8$, they find that the stability curve is independent of density variation in the range $10 < n_H < 10^{11} \text{ cm}^{-3}$.

Hess et al. (1997) address the discrepancy that the physical properties inferred from observations of some low-mass X-ray binaries and Seyfert galaxies correspond to thermally unstable regions of the stability curve predicted by photoionization codes. They have carried out an extensive study of the stability curve as a function of various ionizing continuum and different abundance of the absorbing gas. They have studied the cause of the instabilities in great detail and have cautioned against the outdated fits and parameters used by the simulation code and also against the accuracy of the atomic data then used for determining the thermal balance.

Komossa & Meerschweinchen (2000) and Komossa & Mathur (2001) have extensively studied the stability curve respectively as a function of ionizing continuum and chemical composition of the absorber with the aim of explaining the WA in various narrow line Seyfert 1 galaxies. They find that steeper ionizing continuum stabilizes WA and super-Solar metallicity of the gas enhances the possibility of multiphase WA. By modeling the observations of NGC4051, indications are found that the WA in this object has super-Solar abundance.

4.3 Comparison with earlier work: importance of updated atomic data

In the WA temperature range $10^5 < \log T < 10^7$ K cooling processes are dominated by collisional recombination which can be radiative or dielectronic. These processes lead to local regions of thermal stability in this otherwise unstable temperature range as discussed by Gehrels & Williams (1993), Hess, Kahn & Paerels (1997) and also depicted by RF95. We can see these effects in our

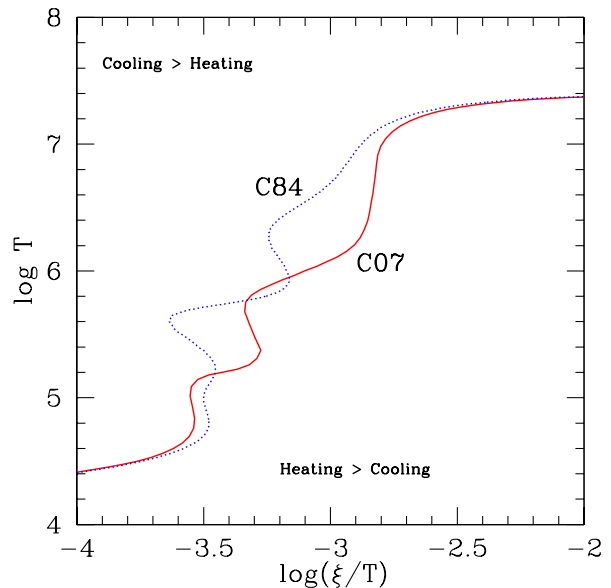


Figure 2. Stability curves showing the distribution of equilibrium temperature T as a function of $\log(\xi/T)$. It is assumed that an optically thin shell of gas of solar metallicity is ionized by a continuum with energy $\xi = 0.8$, extending from 13.6 eV to 40 keV. The regions of the plane where heating or cooling dominates are indicated. The solid curve is obtained using version C07 of *CLOUDY* while the dotted curve is for version c8412a. The *Early set* of parameters, as described in the text, is used in generating the two curves, which are seen to be significantly different for $10^{4.6} < \log T < 10^7$ K.

stability curve generated using the *Early set* of parameter values and shown as the solid curve in Figure 2. However the atomic physics data base has been updated considerably over the last decade and our results show significant quantitative variations from earlier work which we emphasise by making explicit comparisons with RF95.

The dotted line in Figure 2 is a reproduction of the stability curve (using version C8412a of *CLOUDY*) in Figure 3 of RF95 where they had used the *Early set* of physical parameters. The variations in the C07 stability curve from the C84 curve lead to different physical predictions for the WA; for example, the 10^5 K state becomes much more stable in our work resulting in more pronounced possibility of multiphase nature of the WA. The $5 < \log T < 6.5$ region of the stability curve, relevant for WA, sensitively depends on the detailed atomic physics of the various elements which contribute to photoelectric heating and cooling due to recombination and collisionally excited lines. In Paper I we have shown that the total recombination rates (dielectronic + radiative), for the significant cooling agents which bring about the maximum variation in the stability curves in Figure 2, are predicted to be larger in C07 than in C84.

In the WA temperature range $10^5 < T < 10^7$ K, dielectronic recombination dominates over radiative recombination for many ions (Osterbrock & Ferland, 2006). Unlike the radiative recombination rate coefficients, dielectronic recombination rate coefficients (DRRC) have undergone significant changes over the last decade. The importance of revisiting the values of DRRC were first pointed out by Savin et al. (1997) and further emphasised by a series of papers by Badnell and coworkers (Colgan, Pindzola & Badnell 2004, Colgan et al. 2003, Altun et al. 2004, Zatsarinny et al. 2004a, Mit-

Model	Ionizing continuum					Low energy Cut Off	n_H	N_H	Metallicity
	Definition	α_X	s	E_{max}					
<i>Early</i>	Equation 4	0.8	-	-	40 keV	$E_{min} = 13.6 \text{ eV}$ (Equation 4)	10^9 cm^{-3}	Zone 1 (See text)	Z
<i>Standard</i>	Equation 6 Equation 7	0.8	1.2	2.0	200 keV	Equation 7	$10^{11} =$ (See text)	10^{22} cm^{-2}	Z

Table 1. Comparison of the various parameters used to constitute the *Early* and the *Standard* model for stability curves.

nik & Badnell 2004, Zatsarinny et al. 2003, Gu 2003, Zatsarinny et al. 2004b and Gu 2004). The DRRC data base is more extensive now and shows that the rate coefficients for different ionization states of various elements are substantially larger than the values used previously, but the database is still not complete, especially for the lower ionization states. For ions which do not have computed DRRC values, C07 uses a solution, as suggested by Ali et al. (1991); for any given kinetic temperature, ions that lack data are given DRRC values that are the averages of all ions with the same charge. The advantage of this method is that the assumed rates are within the range of existing published rates at the given kinetic temperature and hence cannot be drastically wrong. However, in Paper I, we have checked whether the points in the C07 stability curves have computed DRRC values or guessed average values, concentrating on the parts of the curve which have multiphase solutions for the warm absorber ($10^5 \text{ K} < T < 10^6 \text{ K}$) and are different from the C84 stability curve. We find that all the ions which act as major cooling agents for each of these points in the stability curve have reliable computed DRRC values which are not likely to change in near future. Thus, the new data base provides a more robust measurement of the various physical parameters involved in studying the thermal and ionization equilibrium of photoionised gas. This not only gives us the motivation to improve upon previous qualitative stability curve analysis by various authors (Hess, Kahn & Paerels 1997; Komossa & Mathur 2001; Krolik, McKee & Tarter 1981; Krolik & Kriss 2001; Reynolds & Fabian 1995; Rozanska et al. 2008) but also provides the chance to extend their work with quantitative estimates on the nature of the multiphase WA in Section 8.

4.4 Standard set

The ionizing continuum used in the *Early set* has now been shown by improved spectral UV and X-ray measurements not to correspond to observed continua (Zheng et al. 1997, Shang et al. 2005). As discussed in Section 3, we will use a more realistic SED with two power-law components given by Equation 6 and lower energy cut-off given by Equation 7. The fiducial value for α_X for Seyfert1 galaxies is 1.2 (Netzer 1993). We define a *Standard set* of parameter values to be used in the rest of the paper where the ionizing continuum shown as the solid line in Figure 1 is parametrized by $\alpha_X = 0.8$, $s = 2$ and E_{max} is appropriately adjusted to attain

$\alpha_X = 1.2$. E_{max} for both components is 200 keV. The high energy cut-off is an average of the observational values reported from Beppo-Sax which found hard X-ray spectral cut-off to span the range 50 to 450 keV (Matt 2004; Tueller et al. 2008). The absorbing gas in this *Standard* model is assumed to have solar abundance ($Z = Z_\odot$) as given by Allende Prieto, Lambert & Asplund (2002, 2001), Holweber (2001) and Grevesse & Sauval (1998). The density is given by $n_H = 10^{11} \text{ cm}^{-3}$ as in the *Early set*. In addition we assume $N_H = 10^{22} \text{ cm}^{-2}$, for the slab of the gas in the *Standard set*. Table 1 shows a comparison of the various parameters used in the *Early set* and the *Standard set*.

5 INFLUENCE OF EUV / SOFT X-RAY SLOPE

In this section we consider the effect on the stability curve of changing the shape of the continuum in Equation 6 by varying α_X and s over a range of values. All through the section we assume that the gas has chemical composition of solar abundance.

5.1 Influence of Soft X-ray slope

The left panels of Figure 3 shows the shapes of the ionizing continua and the corresponding stability curves for different values of α_X , s is held at a constant value of 1.2 for these curves. We have highlighted the stable $10^5 \text{ K} < T < 10^7 \text{ K}$ warm absorber states.

For very flat continua, with energy index $\alpha_X \leq 0.2$ or less, almost no stable state exists in the temperature range of $10^5 - 10^7 \text{ K}$, since there are no regions of the curve here with positive slope except for a very narrow one at $\log T \approx 5.6$. The large number of high energy photons pushes the Comptonization temperature to $T > 10^8 \text{ K}$. As noted by Krolik et al. (1981), there is a cooler phase at $\log T < 4.5$ and a hot phase which is transparent to atomic features. Warm absorbers are thus unlikely to be found in AGN which have such flat X-ray spectra. Stability curves for steeper incident spectra show additional stable states in the intermediate temperature regime. Curves corresponding to $\alpha_X = 0.5$ and $\alpha_X = 0.8$ are both stable up to $\approx 2.5 \times 10^5 \text{ K}$. The *standard* curve shows one extensive stable state at 10^6 K . We will discuss the effect of multiple phases further in Section 8. For steeper spectra with $\alpha_X = 1.1$, the absorbing gas is predicted to be stable for all T with the Compton temperature now lying at $\log T = 6.9$. The

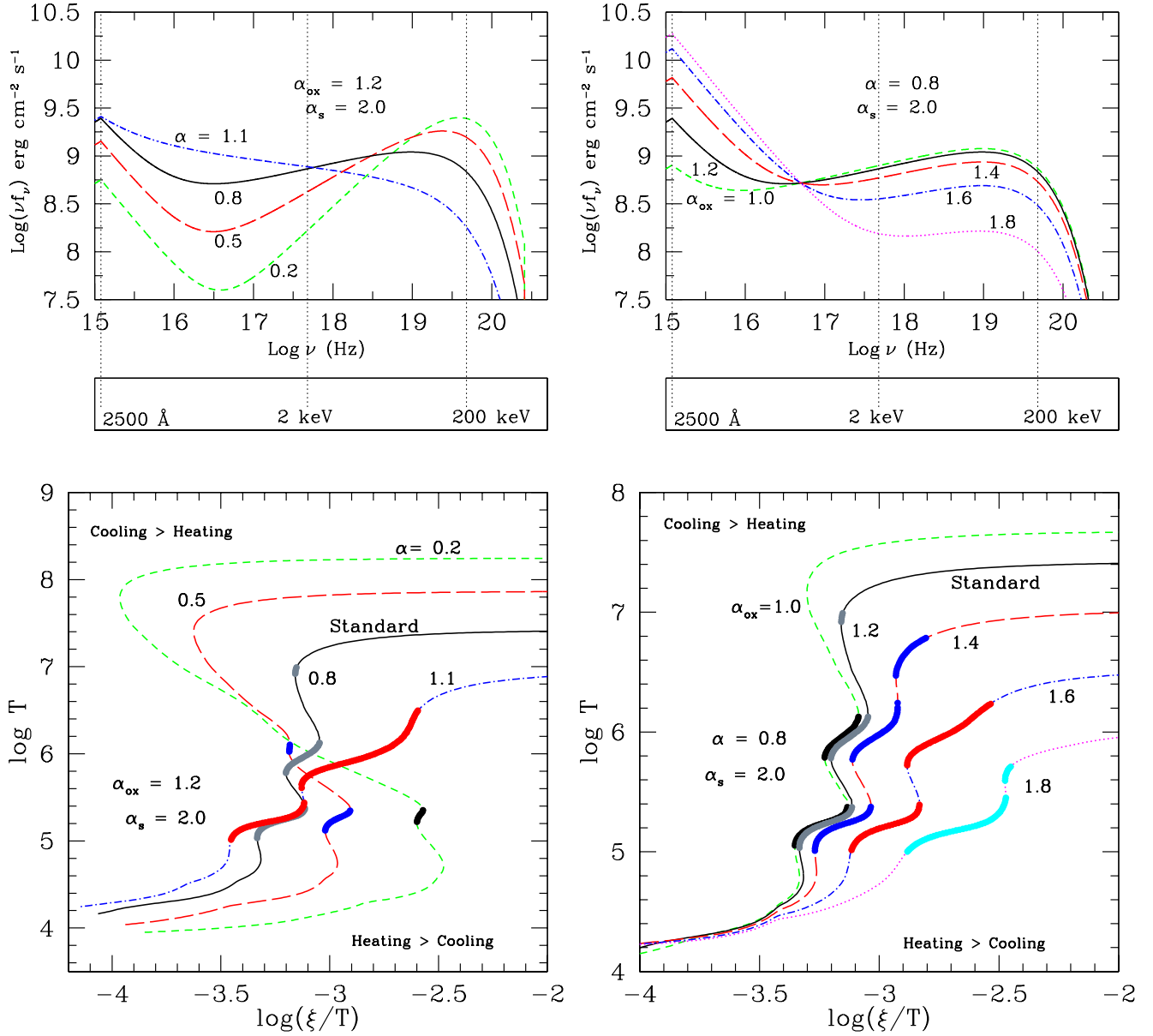


Figure 3. The shapes of the ionizing continua and the corresponding stability curves for varying X-ray slope (left) and varying EUV to X-ray slope, α_{ox} (right) for an optically thin shell of gas of solar metallicity. In the top panels showing the SEDs, the important energy values including the upper energy cut-off (200 keV) and the range of definition for α_{ox} (2500 Å and 2 keV) have been marked and labeled. Left panels: X-ray flux index α is varied from one curve to the other in the range $0.2 < \alpha < 1.1$ with α_{ox} held constant at the value 1.2. Right panels: The EUV to soft X-ray slope α_{ox} is varied over a range of values with the X-ray slope held constant at the standard value 0.8. On the stability curves we have used black on green, blue on red, gray on black, red on blue and cyan on magenta to highlight the stable WA phases. Note that in the left panel, the $\log T$ axis extends up to 9. The flat spectrum ($\alpha = 0.2$) curves have higher temperature Compton stabilization at $T > 10^8$ K.

distinct multiple phases at different temperatures, but in near pressure equilibrium are lost. For such steep continua, stable states exist over a continuous distribution of $\beta = T$ and T in the phase space.

In summary, AGN having flat X-ray spectra with $\alpha < 0.4$ are not likely to have WAs. Although a steeper continuum can lead to physical conditions that can sustain warm absorbing gas in thermal equilibrium, multiphase nature of WA can only be seen for AGN spectra with intermediate slopes of 0.3 . It is interesting to note that multiphase WAs are predicted for continua having slopes in the

range $0.7 < \alpha < 0.9$ which is the observed range for the bulk of the observed AGN population (Wilkes & Elvis 1987; Grupe et al.: 2006; Lopez et al.: 2006).

We would like to note an interesting difference between results obtained by us and that by Krolik & Kriss (2001, hereafter KK01). Using a model ionizing continuum given by Kaspi et al. (2001), KK01 have obtained stability curves computed by version 2.1 of XSTAR (Kallman 2000²). The ionizing continuum by Kaspi et al. (2001) has values of $\alpha_{\text{ox}} = 1.3$ and $\alpha = 0.77$, very sim-

ilar to those used in the *Standard set*. However, KK01 find that the corresponding stability curve shows a steep near vertical rise in temperature from 3×10^4 K to 10^6 K for $40 < \xi < 1500$ which gives a continuous distribution of stable states over a wide range of ξ , while pressure ($\rho = T$) remains almost constant. For the same range of ξ , (50–1200), our *Standard* curve, shows two distinct WA phases in pressure equilibrium with each other and the change in temperature is gradual and spans a much wider range of $\rho = T$ values.

5.2 Influence of α_{ox}

In the right panels of Figure 3 we have shown the results of varying the EUV to soft X-ray slope α_{ox} (see Equation 5). The X-ray slope α_s is held at a constant value of 0.8. Observations find α_{ox} between 1 and 2 as reported by Strateva et al.: 2005 and Steffen et al.: 2006. They find that there is an anti correlation between α_{ox} and the ultraviolet luminosity L (2500Å) as was first reported by Tananbaum et al. in 1979. We have used the representative values of 1.0; 1.4; 1.6 and 1.8 in addition to the *Standard* value 1.2. The WA phases are highlighted as before.

From Figure 3 we see that the nature of stability in the $\alpha_{ox} = 1$ curve is very similar to that in the $\alpha_{ox} = 1.2$ curve. However, beyond 1.2, with a sharper drop in flux from the EUV to the soft X-ray region, i. e., with steeper value of α_{ox} , there is a gradual increase in the stability of the absorbing gas at 10^5 K, and a gradual shift to higher pressure ($\rho = T$). The $\alpha_{ox} = 1.4$ curve shows three distinct stable states at 10^5 ; 10^6 and 10^7 K in pressure equilibrium with each other. For steeper $\alpha_{ox} = 1.6$; 1.8, stability at 10^5 K is increased. The $\alpha_{ox} = 1.8$ curve shows no unstable states. For such spectra, the WA can have a continuous distribution of pressure and density. The Compton temperature for the stability curves understandably gradually drops from $\log T = 7.7$ for $\alpha_{ox} = 1.0$ to $\log T = 6.0$ for $\alpha_{ox} = 1.8$ as the ratio of EUV to X-ray photons increases and Comptonization is progressively dominated by lower energy photons.

To summarise, the existence of the WA is independent of the EUV to X-ray slope of the ionizing continuum. However, its multiphase nature is influenced by this slope; the steeper the fall of flux from EUV to X-ray (i. e., larger α_{ox} , the lesser is the possibility of finding a multiphase WA.

5.3 Influence of E_{max}

The *Standard set* ionizing continuum is exponentially cut off at $E_{max} = 200$ keV (see Equation 6). Results from the Swift/BAT (Burst Alert Telescope) hard X-ray sky survey (Tueller et al., 2008) show that, of the brightest few dozen AGNs, for which E_{max} can be determined, the lowest value is 40 keV, while some 2/3 of the objects have $E_{max} > 120$ keV, the highest value that BAT can measure. As a result an appropriate value of E_{max} for the *Standard Set* needs to be set well above the *Early Set* value. We adopt $E_{max} = 200$ keV. The high energy cut-off is important in Compton processes and hence in determining the Compton temperature of a stability curve, but is not likely to affect its WA region. However, for the sake of completeness we examine the effect on stability curves of varying the value of E_{max} .

Figure 4 shows the various stability curves drawn using the

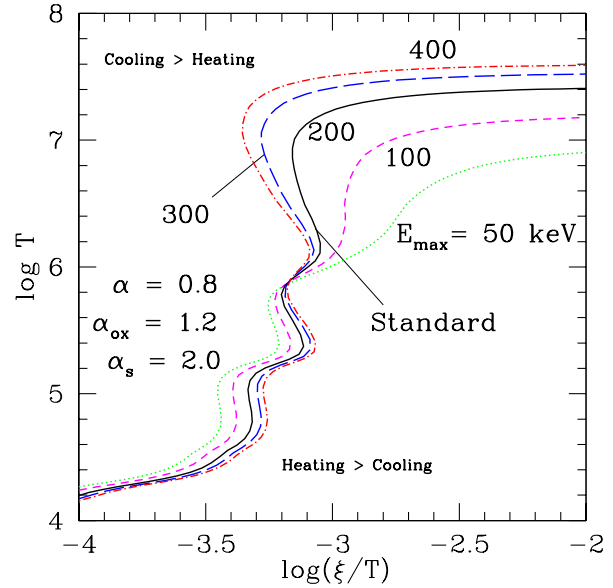


Figure 4. Stability curves drawn using different values for the exponential higher energy cut-off E_{max} . The curves are appropriately labeled. All other physical parameters are same as in the *Standard set*

different values for E_{max} . The curves are appropriately labeled. All other physical parameters are as in the *Standard set*. For the lowest considered value of $E_{max} = 50$ keV, the Compton processes start dominating the thermal balance at lower temperatures resulting in enhanced stability at $T \sim 10^6$ K. However, the influence is still not significant enough to change the overall qualitative nature of the WA or its multiphase properties. The majority of the Swift/BAT AGN have $E_{max} > 100$ keV. For such values of E_{max} , the WA remains effectively insensitive to the variation in the high energy cut-off; the only influence is in increasing the Compton temperature with the increase in E_{max} .

6 INFLUENCE OF DENSITY OF THE ABSORBER

As stated in Section 3, we have assumed that the stability curve is insensitive to the variation in the value of hydrogen density n_H of the WA gas. Based on this assumption, we have taken the liberty to choose an arbitrary fiducial value of $n_H = 10^9 \text{ cm}^{-3}$ for $\xi = 100$, the typical value of ionization parameter reported for WAs, thus yielding $L = R^2 = 10^{11}$ from Equation 1, which we hold constant throughout this paper except in this section. Many authors carrying out photoionization calculations make similar assumptions (Hess, Kahn & Paerels, 1997; Krolik, McKee & Tarter, 1981; Krolik & Kriss, 2001, RF95) and RF95 have even verified this statement over a wide range of densities $10 < n_H < 10^{11} \text{ cm}^{-3}$ for a simple power-law ionizing continuum with $\xi = 0.8$. However, more recently, Rozanska, Kowalska & Goncalves (2008) showed that the stability curve shows remarkable density dependence if the ionizing continuum has a complicated shape with relatively more soft X-ray, photons although the same exercise with a simple power-law ionizing continuum with $\xi = 1.0$ yields no density dependence on the part of the stability curve. In this paper we have studied the stability curve's behaviour as a function of complicated ionizing continua with having different ratios of the soft to hard X-ray photons.

² URL : <http://heasarc.gsfc.nasa.gov/docs/software/xstar/docs/html/xstarmanual.html>.

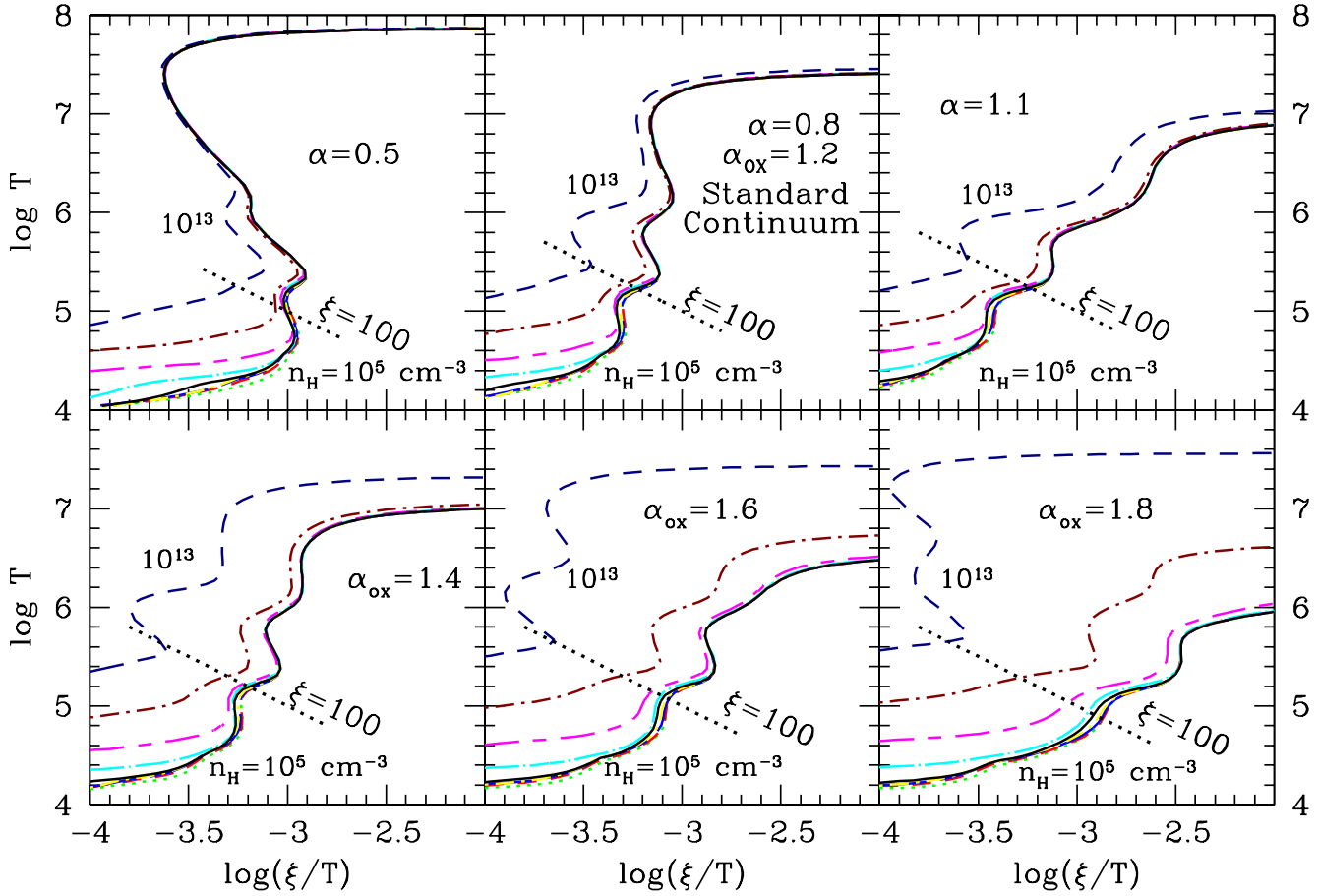


Figure 5. The density dependence of the stability curves as a function of the ionizing continuum. The top panels correspond to the various values of the X-ray slope whereas the bottom panels are for different values of EUV to X-ray slope α_{ox} and all the panels have been appropriately labeled. Density at any point of a stability curve is given by $n_{\text{H}} = (\mathcal{L}=\mathcal{R}^2)^{-1}$. For each ionizing continuum, several stability curves are drawn by varying the ratio $\mathcal{L}=\mathcal{R}^2$ from 10^7 to 10^{15} in multiplicative steps of 10 such that the density at $\xi = 100$ varies from $n_{\text{H}} = 10^5$ to 10^{13} cm^{-3} . The dotted black lines cutting across the curves are the constant $\xi = 100$ lines. In the range $n_{\text{H}} = 10^5$ to 10^{10} cm^{-3} , the density value does not affect the WA range of the stability curve at all. For $n_{\text{H}} > 10^{10} \text{ cm}^{-3}$, the density dependence of the stability curve is seen to increase with the steepness of the ionizing continuum.

Hence it is an interesting exercise to check if the stability curves, especially in the range $10^5 < T < 10^6 \text{ K}$, drawn using the different ionizing continua considered in this paper show any variation if the density is changed.

In this section we relax the assumption made in Section 3 that $\mathcal{L}=\mathcal{R}^2 = 10^{11}$ and for each ionizing continuum considered in Section 5, draw several stability curves by varying this ratio from 10^7 to 10^{15} such that the density at $\xi = 100$ varies from $n_{\text{H}} = 10^5$ to 10^{13} cm^{-3} in multiplicative steps of ten from one curve to another. The results are shown in Figure 5. The upper panels in the figure show the stability curves for continua with different values of the X-ray slope $\alpha = 0.5; 0.8$ and 1.1 , whereas the bottom panels correspond to different values of the EUV to X-ray slope $\alpha_{\text{ox}} = 1.4; 1.6$ and 1.8 . The determination of thermal equilibrium of the WA is seen to be independent of density in the range $10^5 < n_{\text{H}} < 10^{10} \text{ cm}^{-3}$, whatever be the shape of the ionizing continuum. Stability curves with $n_{\text{H}} = 10^{11}$ and 10^{12} cm^{-3} show insignificantly small differences from the rest of the curves with lower densities as we vary α from 0.5 through 0.8 to 1.1. This indicates that the soft X-ray slope has little or no role to play in

inducing density dependence to the estimations of thermal equilibrium conditions. The most interesting result of this exercise is that as the EUV to X-ray slope α_{ox} is increased from 1.2 through 1.4 and 1.6 to 1.8, the WA thermal equilibrium properties become significantly density dependent for $n_{\text{H}} > 10^{11} \text{ cm}^{-3}$ and the dependence is more pronounced with the increase in α_{ox} i.e. with the increase in the relative number of EUV photons. $n_{\text{H}} > 10^{12} \text{ cm}^{-3}$ can be considered to be an upper limit on WA density and would be consistent with clouds residing within the H β broad emission line region, on the scale of the accretion disc, a few thousand Schwarzschild radii (Krongold et al., 2007). Thus higher values of density are unphysical for WA. However, in each of the panels in Figure 5, we have also plotted the $n_{\text{H}} = 10^{13} \text{ cm}^{-3}$ curve for comparison and it shows gross difference from the stability curves with lower densities for all the continuum shapes considered.

Since the $\alpha_{\text{ox}} = 1.8$ curves show the maximum sensitivity to density variation, we select them to investigate the cause of this effect. We choose the $\xi = 100$ model from each of the curves with densities $10^5 < n_{\text{H}} < 10^{13} \text{ cm}^{-3}$ and check what are the dominant heating and cooling agents in determining the thermal

balance. The fractional contribution towards the total cooling rate by the dominant cooling agents undergoes only a gradual change as we change the density though the above mentioned range. The remarkable change is shown by the dominant heating agent. For $n_H = 10^{10} \text{ cm}^{-3}$, the heating agents are all photoionized species and free-free heating starts to dominate for $n_H = 10^{11} \text{ cm}^{-3}$. The percentage of heating by free-free absorption increases from 17 for $n_H = 10^{11} \text{ cm}^{-3}$ to 83 for $n_H = 10^{13} \text{ cm}^{-3}$.

The ionization equilibrium conditions of the absorbing gas can be uniquely determined if the shape of the ionizing continuum and the flux received by the gas is specified. Assuming that the absorber is in ionization equilibrium, *CLOUDY* evaluates the heating and cooling rates at different temperatures for the given gas and determines the thermal equilibrium solution for the temperature where these two rates balance each other. In the WA temperature regime where photoionization is the dominant heating process and thermal equilibrium is achieved by recombination cooling, the temperature estimates become independent of density as both the heating and the cooling terms have similar dependence on density which cancels out from both sides of the thermal balance equation. At higher temperatures, the thermal balance is attained by Compton heating and cooling, in which case also, the density cancels out.

However, the interplay between various heating and cooling processes is also a function of the ionization continuum. For spectral shapes with steep $\propto \nu^{-\alpha}$ there may be sufficiently large number of low energy photons to make the free-free absorption by ionized hydrogen dominate over photoionization as the heating process. The heating rate for this interaction has a different dependence on density and will result in making the thermal equilibrium conditions sensitive to density variations for n_H greater than a certain threshold value.

The interesting point to note at the end of this exercise is that although the mode of photoionization calculations used by us and Rozanska et al. (2008) are different, our results are qualitatively consistent with each other. For sufficiently soft UV dominated ionizing continuum the thermal equilibrium calculations become density dependent if the gas is denser than a certain threshold. Since the gas is also assumed to be in ionization equilibrium, the ionization structure will also be influenced. The effects would be much more pronounced for *constant pressure* mode of calculations as shown by Rozanska et al. (2008). The importance of this result is that for dense gas illuminated by UV dominated ionizing continua, the density of the gas can be estimated directly by modeling the observed spectra in UV.

7 INFLUENCE OF THE CHEMICAL COMPOSITION OF THE ABSORBER

The behavior of the models along the stability curve, from $\log T = 4.0$ to $\log T = 7.0$ is sensitive to the role of atomic physics in determining the thermal state of the gas. The photoionization cross section $\sigma(X^{+i})$ from the ground level of X^{+i} ion with the threshold ϵ_i is given by the equation

$$\begin{aligned} n(X^{+i}) \langle \sigma(X^{+i}) \rangle &= n(X^{+i}) \int_{\epsilon_i}^{\infty} \frac{4J}{h} \sigma(X^{+i}) d\epsilon \\ &= n(X^{+i}) \int_{\epsilon_i}^{\infty} R(X^{+i}) d\epsilon : \end{aligned} \quad (8)$$

where $n(X^{+i})$ is the number density of the X^{+i} ion, $\langle \sigma(X^{+i}) \rangle$ is the number of excitations per particle to the $(i+1)^{\text{th}}$ state and J

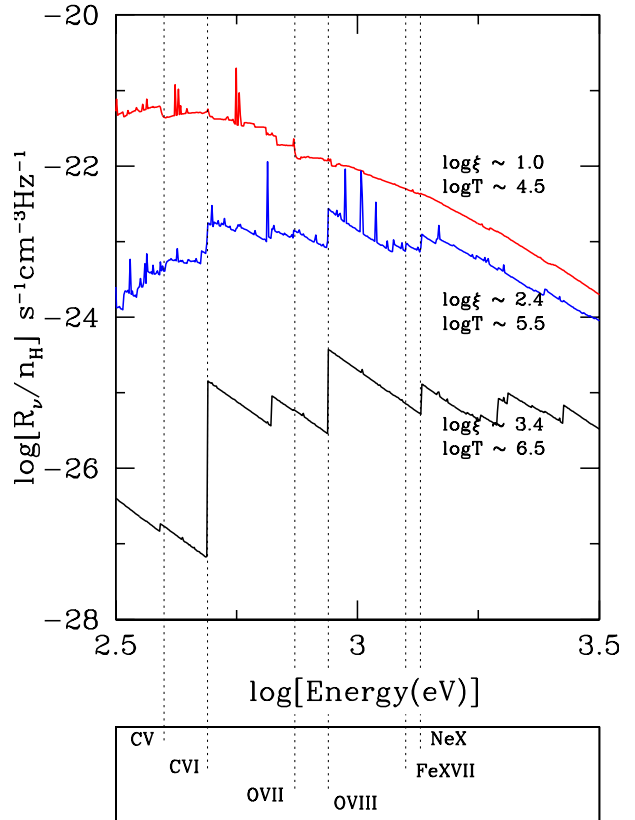


Figure 6. The radiation field interaction rate is plotted as a function of energy for physical models with different ionization parameters chosen from different regions of the standard stability curve. See text for details. The dotted vertical lines mark the absorption edges of some of the ions important for WA, viz. CV, CVI, OVII, OVIII, FeXVII, NeX.

is the mean intensity. Thus the function $R(X^{+i})$ is a measure of the interaction between the radiation field and the X^{+i} ion.

In Figure 6 we have shown the dependence of

$$R = \sum_i R(X^{+i})$$

on $\log \xi$ and hence on the ionization state of the absorbing gas. We have selected three different models along the *Standard* stability curve and plotted R/n_H as a function of energy with the values of $\log \xi$ and $\log T$ indicated for each curve; $n_H = 10^{11} \text{ cm}^{-3}$ being the hydrogen density. The absorption edges of various important ions including CV, CVI, OVII, OVIII, FeXVII and NeX which are the signatures of WA have been indicated with dotted lines. As the gas becomes more ionized by factors of 10 its interaction with radiation decreases by orders of magnitude, especially at energies less than 1 keV. At any given energy the value of R is lower for higher $\log \xi$. However, with highly ionized gas, the interaction shifts to the higher energies. For $\log \xi = 1$, there is no sharp increase in R at energies corresponding to the WA edges; these interactions grow with $\log \xi$ as seen in the middle and the bottom curves corresponding to $\log \xi = 2.4$ and 3.4 respectively.

We see above that at values of $\log \xi$ relevant for WAs, the nature of the interaction between gas and radiation is significantly influenced by the atomic physics of the heavier elements. In the

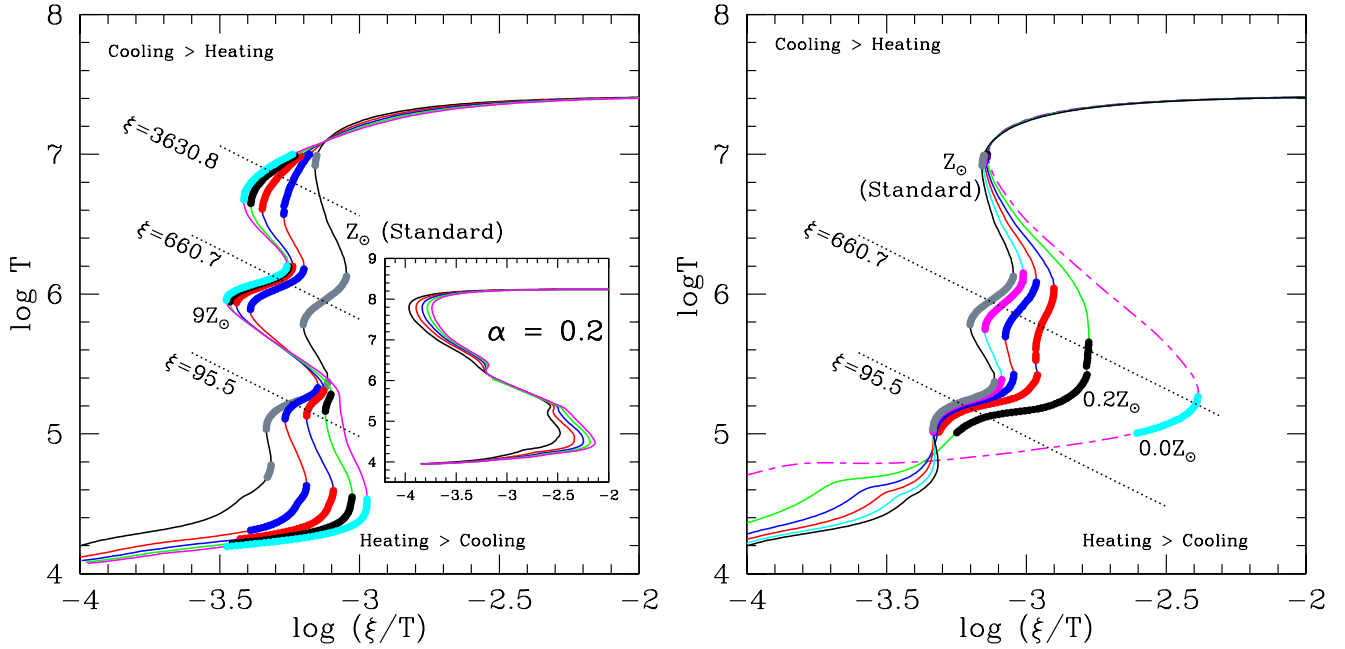


Figure 7. Stability curves for absorbers with different abundances. The left panel shows curves having abundance from Z to $9Z$ in steps of 2. The curves show that absorbers with super-Solar chemical compositions will enhance multiphase nature of the absorber. Except for the curves in the inset window in the left panel, the *Standard set* ionizing continuum with $\alpha = 0.8$ has been used for the calculations. The stability curves in the inset window are, however, obtained using an ionizing continuum with flat X-ray slope of $\alpha = 0.2$ to investigate if enhanced metallicity helps sustain WA for gas irradiated with such flat continuum. The results show no significant stable states in the temperature range $5 < \log T < 7$ for WAs. The right panel shows the curves having sub-Solar abundances from $0.02Z$ to Z in steps of 0.2. Decreases in metallicity are seen to stabilize the curve in the temperature range of 10^5 – 10^6 K. However, the possibility of multiphase media decreases with the decrease in the abundance. In all the panels the stable WA are highlighted as before. The dotted black lines cutting across the stable WA states are constant ξ lines. $\xi = 95.5$ and $\xi = 660.7$ correspond to the middle of the WA states of the *Standard* curve at 10^5 K and 10^6 K respectively and $\xi = 3630.8$ corresponds to the middle of the 10^7 K phase for the $Z=Z_{\odot}$ stability curve.

following subsections we have studied the effect of different chemical compositions of the absorber on the stability curve. The illuminating continuum is assumed to be the same as that in the *Standard set* values (Table 1). We have generated the stability curves for (i) super-Solar abundances, (ii) sub-Solar abundances and (iii) other abundances where specific elements or group of elements have been removed from the solar metallicity.

7.1 Super-Solar Abundance

The left panel of Figure 7 shows stability curves for gas having super-Solar abundances as defined in Hamann & Ferland (1993). In addition to the 10^4 K and the 10^8 K phases, all the curves also exhibit WA states. However the temperatures of the WA phases and their distribution in the phase space change with metallicity. The nature of stability exhibited can be separated into three different groups showing distinctly different trends.

All the curves in the group with solar to three times solar exhibit stable gas at $T \approx 10^5$ K, with the extent of the stable region decreasing as the metallicity is increased. $\xi = 95.5$ for the *Standard* curve, ξ being the ionization parameter corresponding to the middle of the 10^5 K WA phase. The range of ionization parameters for the 10^5 K gas is 50–182 for the *Standard* curve. The $\xi = 95.5$ drawn in the left panel of Figure 7 indicates that the 10^5 K WA is pushed towards higher values of ξ as the metal-

licity increases. Another stable states appears in all the curves at $T \approx 10^6$ K, but this time with the increase in metallicity, the extent of the stable region is increased. $\xi = 660.7$ for the *Standard* curve, where ξ is defined to be the ionization parameter corresponding to the middle of the 10^6 K stable WA phase which shows the range 380–1202 for the *Standard* curve. The solid black line across the 10^6 K phases of the different stability curves is the $\xi = 660.7$ line. Thus, we see that with the increase of metallicity, ξ is decreased slightly and the 10^6 K stable phase moves to lower ξ/T and higher T . A very narrow (in the range of $\log(\xi/T)$) phase is seen to appear at $T \approx 10^7$ K for metallicity of 3 solar. The detailed quantitative comparisons are made in Section 8.

The curves in the next group with $4 < Z/Z_{\odot} < 7$, are very similar to each other, with a very narrow stable state at 10^5 K, which is not in pressure equilibrium with the 10^6 K phase and the 10^7 K state becomes more prominent. As abundances are increased further ($Z/Z_{\odot} > 7$) the stable state at 10^5 K disappears, while the 10^6 K and 10^7 K states remain quite wide and in pressure equilibrium with one another. The stability curves for the super-Solar abundances thus suggest that the possibility for the warm absorbing medium to exist in discrete phases in pressure equilibrium with each other increases with increasing metallicity. We return to these issues in Section 8 with quantitative details.

The stability curves for the super-Solar metallicities with $Z/Z_{\odot} > 3$ are seen to have gas at $T \approx 10^4$ K to be in pres-

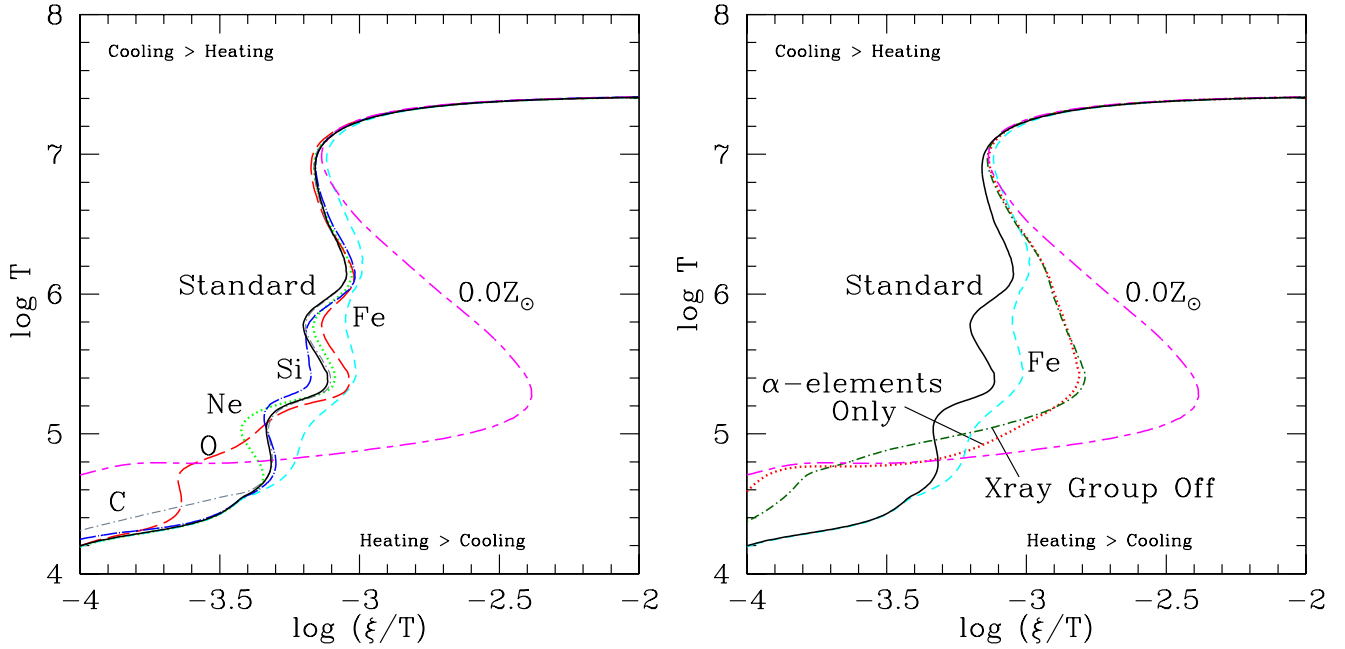


Figure 8. Stability curves for different chemical compositions with certain individual elements or certain groups of elements, as labeled, set to zero. “X-ray Group Off” signifies the absence of the group of metals C, O, Ne, and Fe in the gas abundance, whereas “ α -elements Only” represents an absorbing gas having only α -elements (Ne, Mg, Si, S, Ar, Ca, Ti) as heavy elements. See text for further details. The curve labeled ‘Standard’ in the two panels uses the *Standard* set of values (Table ??). We have also plotted the *zero metals* curve in both the panels for comparison

sure equilibrium with the WA states at higher temperatures. Such stable states at 10^4 K are also highlighted in the corresponding stability curves in the left panel of Figure 7. Gas at 10^4 K might be representing the ‘BELR clouds’. Hence this phenomenon might indicate the interesting possibility of some connection between the X-ray and UV absorber, as discussed by Turner et al.: (1995) and Elvis (2000). However, these results have to be checked out further with more realistic AGN spectra which is beyond the scope of this paper and will be addressed in our next publication (Chakravorty et al., in preparation).

We have also investigated the possibility of high metallicity gas making it possible for WA to exist even when the X-ray ionizing continuum is very flat. The stability curves are shown in the small inset window of the left panel of Figure 7. Even for solar abundance, the $\xi = 0.2$ curves did not show any significant 10^5 K WA and higher metallicity diminishes the chances further. At higher temperatures of 10^6 K, very narrow regions of stability appear for $Z = Z_\odot$. However, even in these cases there is no multi-phase exhibited by the stability curves. Thus even if the gas has high metallicity, WAs are not likely to be present in the intervening medium, if the ionizing continuum is very flat.

7.2 Sub-solar abundance

Gas in AGN has super-Solar metallicity (Hamann & Ferland, 1999). However, AGN illuminate low density gas on large scales which has low abundances, especially at high redshift. Sub-Solar chemical composition are relevant for such line of sight absorbing systems including Damped Lyman- α systems in the inter galac-

tic medium and smaller galaxies like the Magellanic clouds. The inter-cluster medium, for example, has $0.3Z_\odot$ abundance and in certain systems there are even stars with an abundance of $0.01Z_\odot$ (Pettini, 2006 and references therein). It is, therefore, interesting to examine the effects of sub-Solar abundance on the stability curve. We show the low metallicity stability curves in the right panel of Figure 7. As before, the solid black lines across the stable WA phases are the constant ξ lines.

The ionization parameter ξ_5 corresponding to the middle of the 10^5 K stable phase increases from its standard value of $\xi_5 = 95.5$ with the decrease in metallicity and there is gradual enhancement of the thermal stability of gas. On the other hand, with almost constant $\xi_6 = 660.7$, the stable phase at $\log T = 6$ moves towards lower temperature and higher pressure ($\xi = T$) and its extent in the $\log (\xi = T)$ shrinks until such a phase disappears for $0.0Z_\odot$. Detailed quantitative comparisons will be presented in Section 8.

Absorbing gas with *zero metals* might be relevant for super massive black holes (SMBHs) or their seeds at redshift $z > 6$, which are formed by direct collapse and where no star formation precedes the radiating SMBH (Volonteri & Rees, 2005; Begelman, Volonteri & Rees, 2006). We have shown the *zero metals* stability curve in the right panel of Figure 7. There is a single phase WA at 10^5 K with significantly high $\xi_5 = 437$ as compared to the *Standard* $\xi_5 = 95$.

7.3 Influence of individual elements and groups of elements

Figure 6 has shown how the interaction between gas and radiation is sensitive to the ionization potentials of various ions of elements

like C, O, Fe and Ne indicating that the WA states are likely to be affected not only by the overall abundance of the absorber, but also by specific elements and groups of elements. Figure 8 shows the effect on the stability curves if certain elements or groups of elements are not present in the absorbing gas. In both the panels of the figure, we have also drawn the stability curve for the *Standard set* of parameters and *zero metals* for comparison.

The WA consists of absorption edges and lines of different ionization stages of oxygen, carbon, neon and iron. We define the *X-ray group* constituting of only these four elements. The left frame of Figure 8 shows the results of simulating various stability curves corresponding to the removal of different individual elements of the group from a solar composition gas. Setting carbon abundance to zero does affect the stability curve at $\log T < 4.5$ and the deviations imply that Carbon acts as a cooling agent at those temperatures. However at higher temperatures relevant for WA, Carbon has no significant effect. The removal of oxygen and neon leads to deviations in the stability curves which indicate that for $T < 10^5$ K oxygen acts as a significant cooling agent with some contributions from neon, whereas for $T > 10^5$ K both act as heating agents. Removal of iron has the maximum effect as it renders the curve relatively featureless in the range $4.5 < \log T < 7$. Such an effect is expected because at higher energies iron is the most abundant absorbing element and plays a major role to stabilise the gas by acting as a significant heating agent. This result has interesting cosmological consequences. Type Ia supernovae created iron when the Universe was about 1 Gyr old (Hamann & Ferland, 1999 and the references therein). Hence there would be an interesting transition in the nature of the WA at this age; WAs devoid of iron from before this era cannot show a significant 10^6 K phase. Future missions like Constellation X might be able to detect such a change. Like the removal of iron, the removal of the *X-ray group* (O, C, Ne, Fe) as a whole also *flattens* out the stability curve, but to a larger extent as shown in the right panel of Figure 8. If the absorbing system is devoid of the *X-ray group*, the stable states at 10^5 K are pushed towards higher values of ξ with $\xi = 158$ as compared to $\xi = 95$ for the *Standard* curve and there are no higher temperature stable states thus nullifying the possibility of multiphase WA.

In addition to the elements of the *X-ray group*, it is instructive to study the effect of the α -elements (Ne, Mg, Si, S, Ar, Ca, Ti) produced together with oxygen in type II supernovae which precede the type Ia supernovae where iron and associated elements are formed. Thus the relative abundance of these elements gives a handle on the stellar evolution history and the age of the galaxy. Ne is the only α -element which has been studied as a part of the *X-ray group* (O, C, Ne, Fe) as well, and its effect on the stability curve has already been discussed above. Among the remaining α -elements, magnesium, sulphur, argon, calcium and titanium have negligible effects. Only silicon is a significant cooling agent at $\log T \approx 5$, so that removal of silicon shows an almost vertical jump from 10^5 K to 10^6 K in the corresponding stability curve in the left panel of Figure 8. As a group however, α -elements suggest interesting consequences. According to the evolution history of metals in the Universe, the α -elements are formed first, followed by the other metals in subsequent stages. Hence we investigated the nature of an absorbing gas which has only the α -elements as metals and the corresponding stability curve is shown in the right panel of Figure 8 labeled as ' α -elements Only'. For $\log T \geq 5.2$ the curve is same as the "*X-ray group removed*" curve and at lower temperatures, $\log T < 4.5$, it traces the $0.0Z_\odot$ curve. These results suggest that a certain amount of evolution of metals is necessary for any

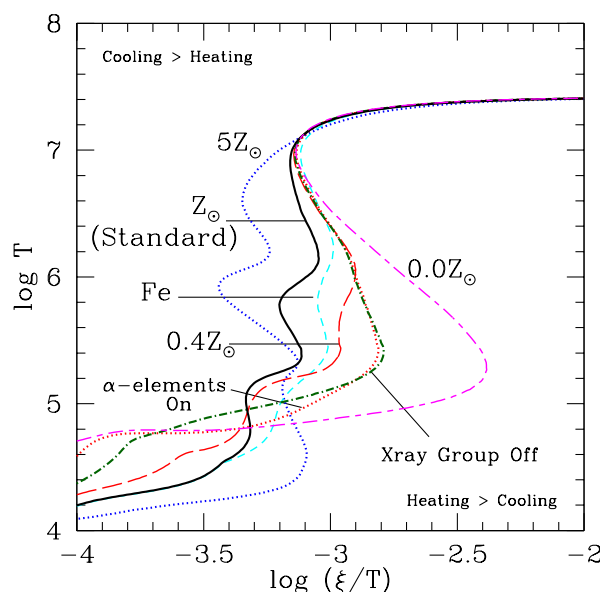


Figure 9. A summary plot depicting the stability curves for a range of chemical compositions. The curves marked 'Fe' and 'X-ray Group Off' correspond to absorbers where iron and the X-ray group elements respectively are absent. An absorber with a composition where only the α -elements are present as the metals, is represented by the stability curve labeled with ' α -elements On'. There is a gradual flattening of the stability curve as one moves from $5Z_\odot$ to $0.0Z_\odot$.

absorbing systems to show WA signatures and might set an upper limit to the redshifts at which warm absorbers can form.

7.4 Summary of abundance effects on stability curves

In Figure 9 we have collected the curves showing the major effects due to varying the chemical composition of the absorber. As the metallicity of the absorber is decreased from $5Z_\odot$ to Z_\odot and to $0.4Z_\odot$, the stability curve flattens gradually. The possibility of finding multiphase WA decreases with decrease in metallicity. This result is in conjunction with those found by Komossa and Mathur (2001). It also decreases if the absorbing medium is deficient in some elements. If a WA lacks iron, but has all the other elements with solar abundance, it then has nearly the same stability properties as an absorber with half solar abundance. The X-ray group of elements are the most influential in making multiple phases possible. Absorbing gas at early epochs of star formation when only α -elements formed show the same thermal properties as absorbers devoid of the X-ray group of elements, thus suggesting that the properties of WA are significantly dependent on the evolution history of metals in the Universe. Figure 9 also shows the stability curve for $0.0Z_\odot$; such a primordial gas of hydrogen and helium has a single phase of absorbing gas at 10^5 K for a significantly high ionization parameter. No stable state at 10^6 K and hence no multiphase solutions are possible if the metallicity of the absorber is $< 0.2Z_\odot$. Metals thus seem to be necessary for absorbing gas to exist at $10^5 \text{ K} < T < 10^7 \text{ K}$.

Hess et al. (1997) have carried out an extensive study trying to account for the unstable thermal equilibrium zones in temperature ranges relevant for AGN and X-ray binaries paying attention to even individual ions of various metals responsible for causing the

instabilities. They have predicted the ionization structure and thermal states of absorbers with a wide variety of chemical compositions. The results posed in this paper especially in Section 7.3 agree qualitatively with their results but as expected, they vary in quantitative details. For example, like them, we also find oxygen and iron to be playing crucial roles in the ionization and thermal balance equations. However, unlike Hess et al. in this paper we find that oxygen and iron influence distinctly different temperature zones of the stability curve. As mentioned in their paper, such minute details would crucially depend upon the accuracy of the atomic physics incorporated which is definitely addressed much better in the current photoionization codes than in 1997.

The determination of the particular ions responsible for the heating or cooling of the gas at WA temperatures, is very sensitive to the exact shape of the ionizing continuum between 50 to 500 eV. Such investigations and quantitative comparisons are beyond the scope of this paper and will be addressed in our subsequent publications (Chakravorty et al. , in preparation).

8 MULTIPHASE ANALYSIS

The equilibrium curves we have derived in the previous sections often contain segments that allow phases at different temperature to occur at similar pressure $\neq T$. This has clear physical interest as distinct phases in pressure equilibrium have been derived in a number of cases of WAs (Krongold et al.; 2003, 2007, Netzer et al.; 2003), while in others it has been claimed that there is a continuous range of ionization parameter (Ogle et al.; 2004, Steenbrugge et al.; 2005). In this section we quantify the extent of these multiphase regions. However, we would like to note that for carrying out such an exercise, the atomic database needs to be accurate. As mentioned a number of times in the previous sections, care has been taken to upgrade the underlying atomic physics in `CLOUDY` with the most recent updates.

In Table ?? we present detailed quantitative estimates of the WA properties for the various parameter sets used in this paper. For convenience of representation we introduce a few definitions for use in Table ?. The first four columns describe the parameter set used to derive the stability curve and the WA properties. n in columns 5, 9 and 13 and T_n in columns 6, 10 and 14 respectively are the ionization parameter and the temperature corresponding to the middle of the 10^n K stable WA phase, where T_n is expressed in units of 10^n K. $\log(\neq T)$ in columns 7, 11 and 15 give the range of $\log(\neq T)$ over which stable states of WA are exhibited for a temperature of 10^n K. For WA to exist in discrete multiphase phases, different temperature stable states require to exhibit the same values of $\neq T$. The larger the range of these common values, higher we presume to be the probability of a multiphase WA. Such intersection in the range of $\neq T$ is represented by $_{56} \log(\neq T)$ for 10^5 K and 10^6 K phases and by $_{67} \log(\neq T)$ for the states at 10^5 K and 10^6 K and their values are noted in columns 8 and 12 respectively. N_p in the second last column is the number of stable states in the stability curve in the temperature range $5 \log T - 7$ and the number of states in pressure equilibrium with each other is given by N_{mp} in the last column. We would note that the values of the various quantities recorded in Table ?? are useful for understanding trends in the variation of the physical quantities as the parameter sets are changed. However, for more robust estimations of these numbers and specific predictions of the WA properties, we require more detailed modeling of the ionizing continuum and the

gas abundances. Such investigations will be described in a subsequent publication (Chakravorty et al. in preparation).

In Figure 10, we plot $_{n} \log T$ against $_{n} \log(\neq T)$ for a range of continuum shapes (left) and abundances (right), where $_{n} \log T$ and $_{n} \log(\neq T)$ are the range of T and $\neq T$ for the stable states at 10^n K. Presumably, the higher the values of these two quantities, the better are the chances of existence of the state at 10^n K, because any perturbed gas is more likely to find a larger stable region. The various parameter sets used to describe WA conditions in this paper have been represented by different symbols which have been explained in the bottom panel. The gray square represents the *Standard set* of parameters and the rest of the symbols indicate the changes from it.

From the systematic analysis we can see the following trends:

The variation of soft X-ray slope of the ionizing continuum shows that WAs exist only if > 0.2 and will have higher temperature gas if > 0.5 .

Increases in the soft X-ray slope decrease the ionization parameter of the 10^5 K WA while decreasing its temperature, but increases both $\neq T$ and T for the 10^6 K phase. Both $_{56} \log(\neq T)$ and $_{67} \log(\neq T)$ increases with the value of $_{\alpha}$, which is also demonstrated by the *square* data points in the top and the middle left panels of Figure 10 accompanied with increase in $_{n} \log T$, indicating that WA phases stabilise with steeper soft X-ray continua.

The Multiphase scenario, however, is not facilitated significantly with the variation in $_{\alpha}$. Multiphase solutions at 10^5 and 10^6 K are seen only for the standard value of $\neq T = 0.8$. Although the $\neq T = 1.1$ stability curve also shows 2 phases, the value of $_{56} \log(\neq T)$ is very low, making the possibility of multiple phases in equilibrium seem unlikely.

We have found very interesting difference between our results and those obtained by Krolik & Kriss (2001). They have drawn stability curves for ionizing continuum having properties similar to our *Standard set* SED having $_{\alpha} = 1.2$ and $\neq T = 0.8$. The stability curves shown in KK01 have a near vertical jump in temperature from 3×10^4 to 10^6 K as $\neq T$ runs from '40 to '1500 thus exhibiting a continuous distribution of stable states in $\neq T - T$ space. For the same set of parameters (ie, the *Standard set*) we not only get two distinct WA phases in pressure equilibrium with each other, but also do not see any drastic change in temperature over a narrow range of $\log(\neq T)$, although our $\neq T$ values also run from '50 to '1200.

As the value of the UV-X-ray slope $_{\alpha}$ is increased, the ionization parameter for the 10^5 K WA increases steadily accompanied by a small decrease in temperature. $_{67} \log(\neq T)$ also increases but with a small increase in temperature.

The range $_{56} \log(\neq T)$ remains almost constant for $_{\alpha} = 1.6$, but abruptly increases for the value of 1.8. $_{67} \log(\neq T)$ grows abruptly for $_{\alpha} = 1.6$ before which it increases steadily but slowly with the increase in $_{\alpha}$. There is no significant WA state at 10^5 K for $_{\alpha} = 1.8$, Comptonization becomes the dominant heating and cooling processes at these temperatures for such an SED. The triangles in the left panels of Figure 10 show these trends.

Multiphase solutions at 10^5 and 10^6 K are seen in the range $1 \leq_{\alpha} \leq 1.6$. For $_{\alpha} = 1.4$, there is an additional stable state at 10^7 K, but $_{67} \log(\neq T)$ is very low to claim any possibility of this state being in pressure equilibrium with the lower temperature phases.

Through the increase of metallicity of the absorbing gas from $0.2Z$ to $9Z$, the 10^5 K WA maintains almost constant tempera-

Physical parameters				Warm absorber properties											
α_{ox}	α	$Z(Z_{\odot})$	Description	ξ_5	T_5	$\Delta_5[\log(\xi/T)]$	$\Delta_{56}[\log(\xi/T)]$	ξ_6	T_6	$\Delta_6[\log(\xi/T)]$	$\Delta_{67}[\log(\xi/T)]$	ξ_7	T_7	$\Delta_7[\log(\xi/T)]$	N_p
1.2	0.8	1.0	<i>Standard set</i>	95	1.67	0.22	0.1	661	0.89	0.15	-	-	-	-	2
1.2	0.2	1.0	Variation of α	-	-	-	-	-	-	-	-	-	-	-	0
1.2	0.5	1.0		182	1.73	0.11	-	-	-	-	-	-	-	-	1
1.2	0.8	1.0		95	1.67	0.22	0.1	661	0.89	0.15	-	-	-	-	2
1.2	1.1	1.0		87	1.66	0.34	0.01	1514	0.97	0.53	-	-	-	-	2
1.0	0.8	1.0	Variation of α_{ox}	91	1.67	0.22	0.1	631	0.9	0.14	-	-	-	-	2
1.2	0.8	1.0		95	1.67	0.22	0.1	661	0.89	0.15	-	-	-	-	2
1.4	0.8	1.0		110	1.63	0.23	0.08	955	0.95	0.19	0.007	5754	0.45	0.13	3
1.6	0.8	1.0		165	1.6	0.28	0.05	1820	0.95	0.35	-	-	-	-	2
1.8	0.8	1.0		347	1.55	0.41	-	-	-	-	-	-	-	-	1
1.2	0.8	0.2	Variation of sub Solar metallicity	158	1.5	0.47	0.002	602	0.36	0.008	-	-	-	-	2
1.2	0.8	0.4		120	1.63	0.35	0.006	692	0.61	0.06	-	-	-	-	2
1.2	0.8	0.6		105	1.65	0.28	0.03	724	0.77	0.11	-	-	-	-	2
1.2	0.8	0.8		95	1.64	0.25	0.06	724	0.86	0.14	-	-	-	-	2
1.2	0.8	1.0		95	1.67	0.22	0.1	661	0.89	0.15	-	-	-	-	2
1.2	0.8	1.0	Variation of super Solar metallicity	95	1.67	0.22	0.1	661	0.89	0.15	-	-	-	-	2
1.2	0.8	3.0		99	1.67	0.12	0.07	549	1.1	0.19	0.07	3630	0.63	0.09	3
1.2	0.8	5.0		114	1.68	0.06	-	524	1.15	0.2	0.11	3311	0.67	0.14	3
1.2	0.8	7.0		125	1.64	0.02	-	501	1.16	0.21	0.13	3162	0.69	0.16	2
1.2	0.8	9.0		-	-	-	-	501	1.18	0.22	0.15	3162	0.72	0.17	2

Table 2 The physical and thermal stability properties of WAs corresponding to various parameter sets considered in this paper. The various physical properties for the WA are given in columns 1 - 4. Columns 5 - 7 note the presence of the different components of the WAs at $T \sim 10^5, 10^6$, and 10^7 . The number of WA phases is given by column 8 while a qualitative discussion of the WA is given in column 9.

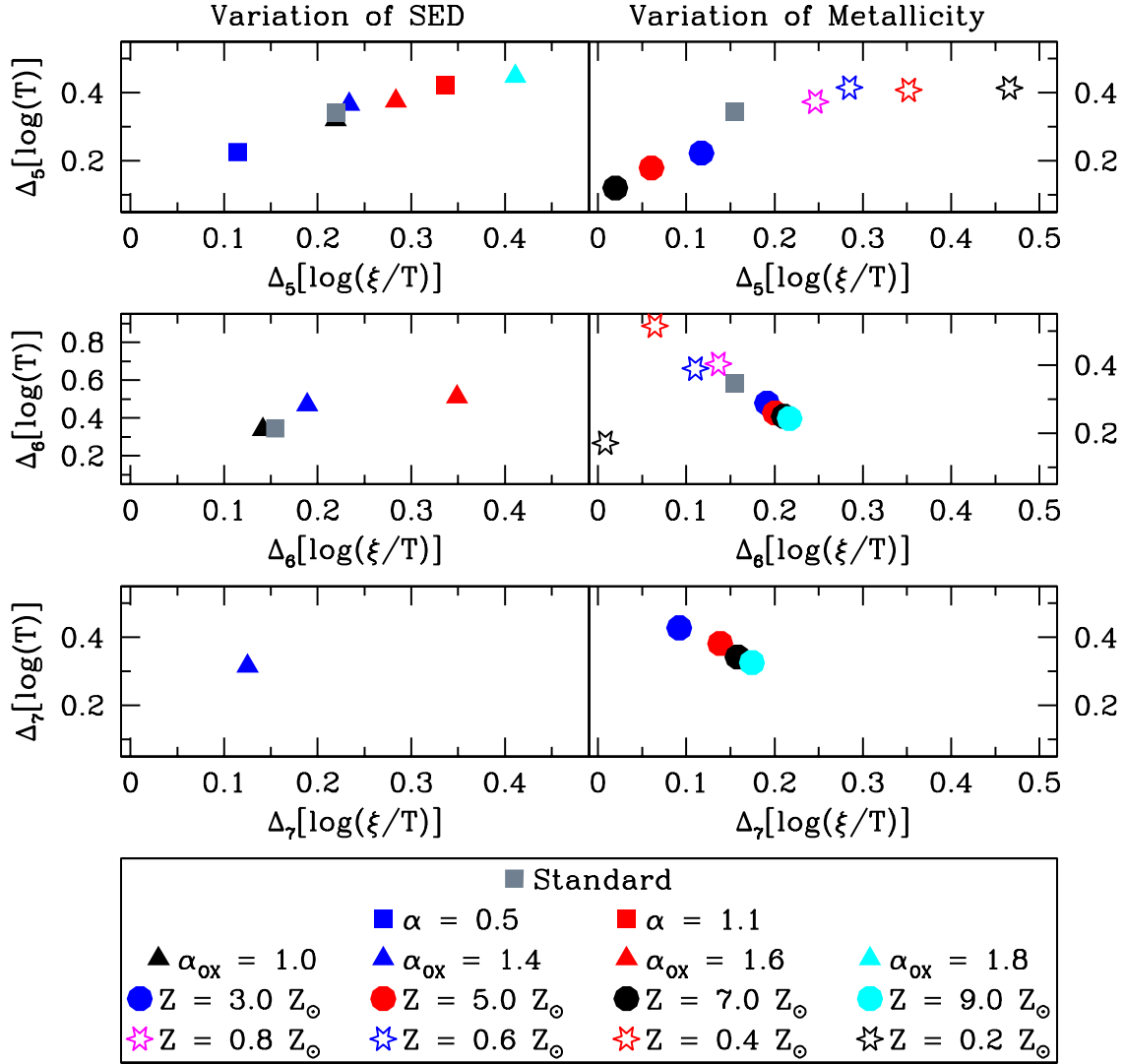


Figure 10. For the stable states of the WAs we have plotted $\Delta[\log(T)]$ against $\Delta[\log(\xi/T)]$ and have considered the parameter sets where we have varied the SED of the ionizing continuum and the metallicity of the absorbing gas. See text for details. Various symbols used to identify the different parameter sets used in this paper, are explained in the bottom panel. The gray square represents the *Standard parameter set* and for the others the deviations from that set are mentioned.

ture. For sub-Solar metallicity, Δ_5 decreases steadily through the increase of abundance, but this trend is inverted for super-Solar metallicity. The 10^6 K WA, on the other hand, shows a rise in temperature T_6 throughout the metallicity variation, while Δ_6 remains constant within a factor of 1.4.

There is an anti-correlation between $\Delta_5[\log(\xi/T)]$ and $\Delta_6[\log(\xi/T)]$; the 10^5 K WA shrinks in $\log(\xi/T)$ until it vanishes for $9Z_\odot$, whereas the phase at 10^6 K progressively grows in $\log(\xi/T)$ from $0.4Z_\odot$ to $9Z_\odot$. This trend is also depicted in the top and the middle right panels of Figure 10 by the *open stars* and the *closed circles*. A 10^7 K phase starts appearing from $3Z_\odot$, and $\Delta_7[\log(\xi/T)]$ increases with abundance.

Interesting multiphase properties are exhibited by WA with varying abundance. $\Delta_5[\log(\xi/T)]$ is significant in the range $0.4Z_\odot$ to $3Z_\odot$ for which 10^5 and 10^6 K gas are in pressure equilibrium with each other. Beyond this range for $Z > 3Z_\odot$,

the stability curves show the interesting feature of significant multiphase solution between the 10^6 and 10^7 K phases; a property depicted by only these three stability curves among all the parameter sets considered in this paper.

In the case of the parameter sets having super-Solar metallicity, we find an interesting phenomenon depicted by the stability curves. For $Z = 3Z_\odot$, the WA stable phases ($5 < \log T < 7$) are seen to be in pressure equilibrium with gas at 10^4 K, which might be representing the ‘broad emission line region (BELR) clouds’. Such a feature in the stability curve might indicate the connection between the X-ray and UV absorber.

9 SUMMARY

Absorption edges due to various partially ionized elements are seen in the soft X-ray spectra of about half of the Seyfert1 galaxies and observed quasars. These absorption features are due to the presence of a warm ($10^5 - 10^{6.5}$ K) gas along our line of sight to the AGN. We have shown that the existence and nature of this absorption component crucially depends on the shape of the ionizing continuum from the central source which illuminates the gas, and also on the chemical composition of the absorbing medium. We have used the stability curve as a tool to study the stability of the WA as a function of its various physical properties.

We have considered an ionizing continuum with two power-law components which together reproduce the observed X-ray spectral index as well as the observed values of α_{ox} . Systematic investigation shows that if the X-ray spectral index, α , of the ionizing continuum intervening gas of solar metallicity is flat with $\alpha \approx 0.2$, then the AGN cannot have a WA. For moderately steep X-ray spectra with $0.5 \leq \alpha \leq 1.1$, it is possible to sustain a WA. A multiphase nature of the WA is, however, seen only for $\alpha \geq 0.8$. It is an interesting coincidence that most of the observed quasars also have soft X-ray slopes similar to $\alpha \approx 0.8$ and in future studies we shall investigate whether such a coincidence leads to deeper physical implications. If the ionization continuum becomes even steeper then, instead of discrete phases, the absorbing gas exhibits a continuous distribution of $\alpha = T$ and T . We have also verified that the nature of the WA is not affected by the higher energy cut-off of the ionizing continuum.

Temperature estimates for warm absorbing gas were generally accepted to be independent of the density of the gas, because the ionization and thermal equilibrium is believed to be achieved by the balance between photoionization and recombination. We show in this paper, in agreement with Rozanska et al. (2008), that the stability properties of highly dense WA might show density dependence influenced by sufficiently soft UV dominated ionizing continuum. This is a very interesting result because it implies that for such objects, we would not require independent estimates of density from observations; modeling the UV spectra itself can provide constraints on gas density.

The chemical composition of the absorbing medium plays a critical role in determining its multiphase nature. The higher the metallicity of the medium, the greater is the probability of a multiphase parameter space. The role of individual elements or certain important groups of elements were also studied. Amongst the elements, iron, which is formed from type Ia supernovae no earlier than 1 Gyr, plays the most important role as a heating agent at higher temperatures (10^5 K) while oxygen is a significant cooling agent for $T \approx 10^5$ K. The X-ray group (C, Ne, O, Fe), understandably, has significant influences, because the constituent elements are the ones which have important atomic transitions in the energy range relevant for warm absorbers ($0.3 - 1.5$ keV). If the absorber is over abundant in iron, oxygen or in the X-ray group of elements then the absorbing medium is likely to be multiphase. A very interesting result seems to suggest itself from the study of influence of α -elements (Ne, Mg, Si, S, Ar, Ca, Ti), which are the first metals formed in the Universe along with oxygen through the supernovae of type II. The thermal properties of the warm absorber change drastically from the time when the absorbing gas is essentially constituted of only α -elements as metals to the time when the absorber is enriched enough to have the whole X-ray group included in its chemical composition. We have also observed that zero metal abundance gas does not produce WAs in AGN. Our anal-

ysis on the chemical composition of the absorbing gas shows that the warm absorber temperature range is very sensitive to the exact abundance of the absorber and there is an indication that the warm absorber might have super-Solar metallicity. While fitting soft X-ray data and determining the physical properties of the warm absorber in individual objects care should be taken to include the effect of super-Solar metallicities.

When we consider super-Solar metallicity, the stability curve shows a 10^4 K stable state is in pressure equilibrium with the WA stable phases. This might imply some connection between the WAs and the BELR. We plan to take up this issue in future work.

We have used an upgraded version of `CLOUDY` (C07.02) where the most recent developments in atomic physics have been incorporated. This gives us the confidence to carry out a quantitative analysis on the multiphase nature of the WA presented in rigorous details in Section 8. We have been able to provide specific trends of the behaviour of the WA as a function of the prevalent physical conditions like the shape of the ionizing continuum and the chemical composition of the gas. Comparison between observations of WA properties and simulations can be made more concrete by providing such quantitative measures. We will extend this exercise to greater details in our subsequent publications.

In this paper we have used simple broken power-laws to define the ionizing continuum for the absorbing gas. However, the soft excess in Ultraviolet is often modeled using blackbody components which peak at $T \approx 150$ eV. Moreover the continuum spectra of AGN also has the disk blackbody component at 20 eV $\leq T \leq 30$ eV. We intend to investigate the effects of such continua on the WA properties as the next step in this systematic analysis.

ACKNOWLEDGEMENTS

SC would sincerely like to thank Ranjiv Misra and Raghunath Sri-anand for useful discussions and for suggestions which have helped the development of the paper. We would like to sincerely thank the anonymous referee whose comments have significantly improved the paper.

REFERENCES

- Ali, B.; Blum, R. D.; Bumgardner, T. E.; Cranmer, S. R.; Ferland, G. J.; Haefner, R. I. & Tiede, G. P., 1991, *PASP*, 103, 1182
- Allende Prieto, C., Lambert, D.L., & Asplund, M., 2001, *ApJ*, 556, L63
- Allende Prieto, C., Lambert, D.L., & Asplund, M., 2002, *ApJ*, 573, L137
- Altun Z., Yumak A., Badnell N. R., Colgan J., Pindzola M. S., 2004, *A&A*, 420, 775
- Ashton, C. E., Page, M. J., Branduardi-Raymont, G., Blustin, A. J., *MNRAS*, 366, 521 (2006)
- Begelman, M.C., Volonteri, M., Rees, M.J. 2006, *MNRAS*, 370, 289
- Blustin, A. J. et al: 2003, *A&A*, 403, 481
- Blustin, A. J.; Page, M. J.; Fuerst, S. V.; Branduardi-Raymont, G. & Ashton, C. E., 2005, *A&A*, 431, 111
- Chakravorty, S., Kembhavi, A.K., Elvis, M., Ferland, G. & Badnell, N.R., 2008, *MNRAS*, 384L, 24
- Colgan J., Pindzola M. S., Whiteford A. D., Badnell N. R., 2003, *A&A*, 412, 597
- Colgan, J., Pindzola, M.S. & Badnell, N.R. 2004, *Astron. Astrophys.* 417, 1183
- Collinge, M. J. et al: *ApJ*, 557:2, (2001)
- Crenshaw, D. M., Kraemer, S. B., & George, I. M. 2003, *ARA&A*, 41, 117G
- Dumont, A.-M., Abrassart, A., & Collin, S. 2000, *A&A*, 357, 823
- Elvis, M., 2000, *ApJ*, 545, 63

- Ferland, G. J.; Korista, K. T.; Verner, D. A.; Ferguson, J. W.; Kingdon, J. B. & Verner, E. M., 1998, *PASP*, 110, 761-778
- Field, G.B., 1965, *ApJ*, 142, 531
- Gehrels, N and Williams, E.D., *ApJ* 418:L25, 1993
- George, I. M.; Turner, T. J.; Netzer, Hagai; Nandra, K.; Mushotzky, R. F. & Yaqoob, T., 1998, *ApJS*, 114, 73
- Goncalves, A. C.; Collin, S.; Dumont, A.-M.; Mouchet, M.; Rozanska, A.; Chevallier, L. & Goosmann, R. W., 2006, *A&A* 451, L23
- Grevesse, N., & Sauval, A.J., 1998, *Space Science Review*, 85, 161-174
- Grupe, D.; Mathur, S.; Wilkes, B. & Osmer, P., 2006, *ApJ*, 131, 55
- Gu M. F., 2003, *ApJ*, 590, 1131
- Gu, M. F. 2004, *ApJS*, 153, 389
- Halpern, J.P., 1984, *ApJ*, 281,90
- Hamann, F., Ferland, G., 1993, *ApJ*, 418, 11
- Hamann, F., Ferland, G., *Annu. Rev. Astron. Astrophys.* 1999, 37:487
- Hess, C.J.; Kahn, S.M.; Paerels, F.B.S., 1997, *ApJ*, 478, 94
- Holweger, H., Joint SOHO/ACE workshop Solar and Galactic Composition. Edited by Robert F. Wimmer-Schweingruber. Publisher: American Institute of Physics Conference proceedings vol. 598 location: Bern, Switzerland, March 6 - 9, 2001, p.23
- Kaastra, J. S.; Steenbrugge, K. C.; Raassen, A. J. J.; van der Meer, R. L. J.; Brinkman, A. C.; Liedahl, D. A.; Behar, E. & de Rosa, A., 2002, *A&A*, 386, 427
- Kallman, T. R. 2000, *XSTAR User's Guide*, version 2.1 (Greenbelt, MD: NASA/GSFC)
- Kaspi, S. et al. , 2001, *ApJ*, 554, 216
- Kaspi, S. et al.: 2002, *ApJ*, 574, 643
- Kinkhabwala, A. et al.: 2002, *ApJ*, 575, 732
- Komossa & Mathur 2001, *A&A*, 374, 914
- Komossa & Meerschweinchen 2000, *A&A*, 354, 411
- Krolik, J., & Kriss, G. A. *ApJ* 561:684, (2001)
- Krolik, J. H., McKee, C. F., & Tarter, C. B. 1981, *ApJ*, 249, 422
- Krongold, Y.; Nicastro, F.; Brickhouse, N. S.; Elvis, M.; Liedahl, D. A. & Mathur, S., 2003, *ApJ* 597, 832
- Krongold, Y.; Nicastro, F.; Brickhouse, N. S.; Elvis, M. & Mathur, S., 2005a, *ApJ* 622, 842
- Krongold, Y.; Nicastro, F.; Elvis, M.; Brickhouse, N. S.; Mathur, S. & Zezas, A., 2005b, *ApJ* 620, 165
- Krongold, Y.; Nicastro, F.; Elvis, M.; Brickhouse, N.; Binette, L.; Mathur, S.; Jimenez-Bailon, E., 2007, *ApJ*, 659, 1022
- Mathews, W.G.; Ferland, G.J., 1987, *ApJ*, 323, 456
- Matt, G., *NuPhS*, 132, 97M, 2004
- Mitnik, D.M. & Badnell, N.R. 2004, *Astron. Astrophys.* 425, 1153
- Morales, R., Fabian, A. C. & Reynolds, C. S., *MNRAS*, 315, 149, (2000)
- Murray, N.; Chiang, J., 1995, *ApJ*, 454L, 105
- Nandra, K., & Pounds, K. A. 1994, *MNRAS*, 268, 405
- Netzer, H. 1993, *ApJ*, 411, 594
- Netzer et al.: , 2003, *ApJ* 599, 933
- Nicastro, F.; Fiore, F.; Perola, G. C. & Elvis, M., 1999, *ApJ* 512, 184
- Ogle, P. M.; Mason, K. O.; Page, M. J.; Salvi, N. J.; Cordova, F. A.; McHardy, I. M. & Priedhorsky, W. C., 2004, *ApJ*, 606, 151
- Osterbrock D. E., Ferland G. J., 2006, *Astrophysics of Gaseous Nebulae and Active Galactic Nuclei*, 2nd edn. University Science Books, Sausalito, CA
- Pettini, M., *The Fabulous Destiny of Galaxies: Bridging Past and Present*. Marseille International Cosmology Conference (5 : 2005: Marseille, France) Proceedings of the Vth Marseille International Cosmology conference, June 20-24, 2005, Marseille, France. Edited by V. LeBrun, A. Mazure, S. Arnouts and D. Burgarella. ISBN 2914601190. Paris: Frontier Group, 2006, p.319
- Reynolds, C. S. 1997, *MNRAS*, 286, 513
- Reynolds, C.S. & Fabian, A.C., *MNRAS*, 273:1167 (1995)
- Rozanska, A., Czerny, B., Dumont, A.-M., Collin, S., & Siemiginowska, A. 2004, *ApJ*, 600, 96
- Rozanska, A.; Goosmann, R.; Dumont, A.-M. & Czerny, B., *A&A* 452, 13 (2006)
- Rozanska, A., Kowalska, I. & Goncalves, A.C., 2008, *A&A*, 487, 895
- Savin, D.W. et al. 1997, *ApJL*, 489, 115
- Shang, Z. et al.: 2005, *ApJ*, 619,41
- Steenbrugge, K.C. et al.: *A&A* 434, 569 (2005)
- Steffen, A. T.; Strateva, I.; Brandt, W. N.; Alexander, D. M.; Koekemoer, A. M.; Lehmer, B. D.; Schneider, D. P.; Vignali, C. , 2006, *AJ*, 131, 2826
- Strateva, Iskra V.; Brandt, W. N.; Schneider, Donald P.; Vanden Berk, Daniel G.; Vignali, Cristian, 2005, *AJ*, 130, 387
- Tananbaum, H. et al.: , 1979, *ApJ*, 234, L9
- Tarter, C.B., Tucker, W. and Salpeter, E.E., *ApJ* 156:943 (1969)
- Tueller, J.; Mushotzky, R. F.; Barthelmy, S.; Cannizzo, J. K.; Gehrels, N.; Markwardt, C. B.; Skinner, G. K. & Winter, L. M., 2008, *ApJ*, 681, 113
- Turner, T. J.; Nandra, K.; George, I. M.; Fabian, A. C.; Pounds, K. A. 1993, *ApJ*, 419, 127
- Turner, A. K., Fabian, A. C., Lee, J. C., & Vaughan, S. 2004, *MNRAS*, 353, 319
- Volonteri, M., Rees, M.J. 2005, *ApJ*, 633, 624
- Wilkes, B.J. & Elvis, M., 1987, *ApJ*, 323, 243
- Zatsarinny O., Gorczyca T. W., Korista K. T., Badnell N. R., Savin D. W., 2003, *A&A*, 412, 587
- Zatsarinny O., Gorczyca T. W., Korista K. T., Badnell N. R., Savin D. W., 2004a, *A&A*, 417, 1173
- Zatsarinny O., Gorczyca T. W., Korista K. T., Badnell N. R., Savin D. W., 2004b, *A&A*, 426, 699
- Zheng, W.; Kriss, G.A.; Telfer, R.C.; Grimes, J.P. & Davidsen, A.F., 1997, *ApJ*, 475, 469